JPRS-JST-88-021
23 SEPTEMBER 1988

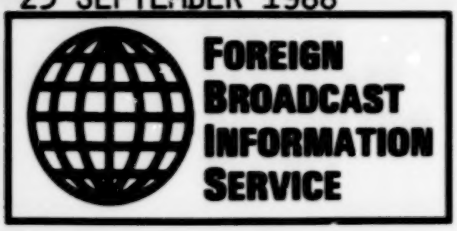

JPRS Report

Science & Technology

Japan

12TH COMPOSITE MATERIALS SYMPOSIUM

JPRS-JST-88-021

23 SEPTEMBER 1988

SCIENCE & TECHNOLOGY

JAPAN

12TH COMPOSITE MATERIALS SYMPOSIUM

43063807 Tokyo DAIJUNIKAI FUKUGO ZAIRYO SYMPOSIUM (KOEN YOSHISHU) in Japanese 22-23 Oct 87

[Selected articles from the 12th Composite Materials Symposium held 22-23 Oct 87 in Tokyo; sponsored by the Japan Composite Materials Society and co-sponsored by the Japan Machinery Society, Japan Metal Society, Japan Aerospace Society, Japan Materials Society, and Reinforced Plastics Society]

CONTENTS

Design, Analysis of Hybrid Laminated Cylinder

43063807a Tokyo DAIJUNIKAI FUKUGO ZAIRYO SYMPOSIUM (KOEN YOSHISHU) in Japanese 22-23 Oct 87 pp 31-34

[Article from day 1, session 8, by Yoshifumi Nakano and Akiko Nakazono, Takatsuki Research Laboratory, Sumitomo Chemical Co., Ltd.]

[Text] **1. Objective**

With the use of CFRP (carbon fiber reinforced plastics) structural materials in many fields in recent years, design and analysis technologies making maximum use of orthotropic characteristics have become important. In this research, the basic structural element was a cylinder, easily formable by the FW method, for which analytic software was developed. This report will present an outline of the software and provide examples of thermal stress and bending analyses.

2. Analysis Method

The analysis method developed by Whitney, et al.,[1] is well known as a program to analyze a laminated cylinder in which various loads work. Our company independently developed a cylinder analysis program called "CYLIN," using the analysis method developed by Whitney, et al., as a reference.[2-12] The cylinder analysis program we developed was based on the following premises.

(1) The shell theory of Vlasov-Ambartsumyan (taking into consideration the thickness direction strain ϵ_z)[7,9] was used for the stress-strain, and the shell theory of Donnell was used for buckling[3,8,10-12]

(2) A cylinder was used in which each layer of the homogeneous and orthogonal anisotropic materials had been bonded in the shape of a concentric circle

(3) The mean radius (R) and thickness (T) were fixed for a thin cylinder of R, L >> t

(4) Microdisplacement: u,v,w<t; Microstrain: ϵ_x, ϵ_y, γ_{xy}, ϵ_z

(5) Shearing strains γ_{xz} and γ_{yz} in the thickness direction were ignored

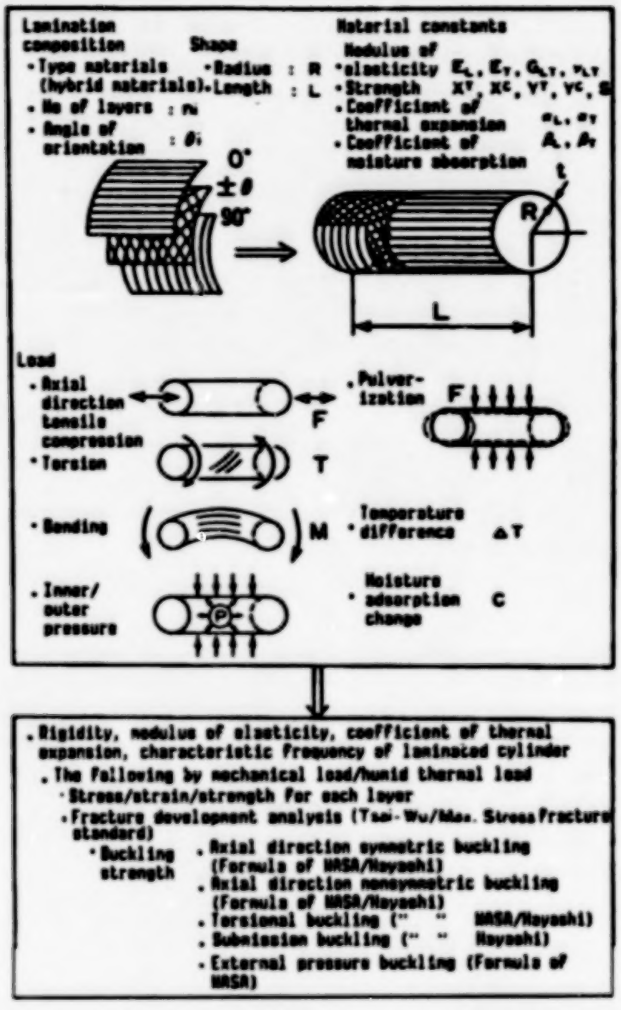

Figure 1. Cylinder Analysis Program "CYLIN"
Premises: Thin cylinder (R, L > T)
Microstrains (ϵ_X, ϵ_Y, γ_{XY}, ϵ_Z)

The functions of this software are shown in Figure 1. All inputs and outputs use conversational and menu selection formats, operations are conducted by a computer, and analysis can be performed easily. Although the stress, strain, and strength computations for the compounding of various loads such as axial direction tension/compression, torsion, bending, internal and external pressures are simple, the following conditional expression was used for the buckling computation.[12]

$$R_C + R_P + R_S{}^2 + R_B = 1$$

Here, stress ratio: R = (generated stress)/(critical buckling stress); C: compression (minus in tension); P: external pressure (minus in internal pressure); S: torsion; B: bending conditional expression $\Sigma R \geq 1$.

The method of decreasing the elastic constants (E_y, G_{xy}, ν_{xy}, etc.) against the fracture mode of the fractured layers was used for fracture progress

analysis. Computations on fracture progress were made independently on the upper surface, lower surface, and side surfaces in the case of bending and pulverizing loads. When there is a matrix fracture even on a portion of the circumference, the elastic constant of the entire layer circumference decreases, so accurate buckling stress computations cannot be expected in the case of buckling by bending. The physical constants of CFRP and ALFRP (alumina fiber reinforced epoxy plastics) used in this computation are shown in Table 1.

Table 1. Mechanical Characteristics of FRP Used in This Calculation

			Unit	1M6/Epoxy	ALF/Epoxy
ρ		Specific gravity		1.6	2.4
V_f		Fiber volume fraction	%	60.0	60.0
Elastic constant	E_x	Fiber direction elastic modulus	kgf/mm^2	16000	12300
	E_y	Elastic modulus in perpendicular direction to fiber	kgf/mm^2	900	1800
	G_{xy}	Shearing elastic modulus	kgf/mm^2	500	1000
	ν_{xy}	Poisson's ratio	kgf/mm^2	0.30	0.29
Strength constant	X^t	Fiber direction tensile strength	kgf/mm^2	250	120
	X^c	Fiber direction compressive strength	kgf/mm^2	150	190
	Y^t	Tensile strength in perpendicular direction to fiber	kgf/mm^2	5	8
	Y^c	Compressive strength in perpendicular direction to fiber	kgf/mm^2	20	20
	S	Shearing strength	kgf/mm^2	8	8
Coefficient of thermal expansion	α_x	Fiber direction coefficient of thermal expansion	10^{-6} K	-0.69	4
	α_y	Coefficient of thermal expansion in perpendicular direction to fiber	10^{-6} K	25	37
	α_z	Thickness direction coefficient of thermal expansion	10^{-6} K	25	37

3. Analysis Result

The computation analysis result on residual stress in the case of molding is shown in Figure 2. The circumference direction residual thermal stress was compared on a two-layer laminated cylinder [0°/90°] and a spiral (alternate) laminated cylinder [$(0°/90°)_3$] which used the orthogonal prepregs of the 90° layer and the 0° layer. The stress value of the spiral

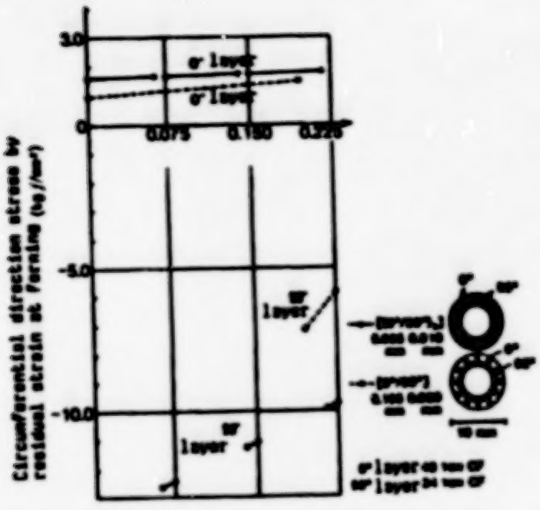

Figure 2. Circumferential Direction Stress by Residual Strain in Case of Forming of $[(0°/90°)_3]$ and $[0°/90°]$ Laminated Cylinder (ΔT = -100°C)

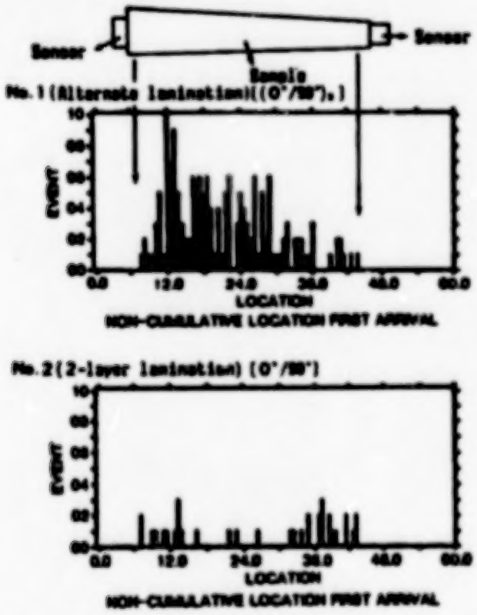

Figure 3. Comparison of Number of AE Events in Case of Temperature Drop of $[(0°/90°)_3]$, $[0°/90°]$

laminated cylinder was approximately two times higher than that of the two-layer laminated cylinder.

The number of acoustic emission (AE) events when the temperature drops in these two types of laminating structures are shown in Figure 3. the number

of events for the spiral laminated cylinder is much greater than that for the two-layer laminated cylinder, and it can be understood that many more matrix cracks are generated by the difference in the thermal expansion coefficient and the drop in temperature. It is considered that one of the reasons why the four-point flexural strength of the spiral laminated cylinder is dispersed in comparison with that of the two-layer laminated cylinder lies in this residual thermal stress.

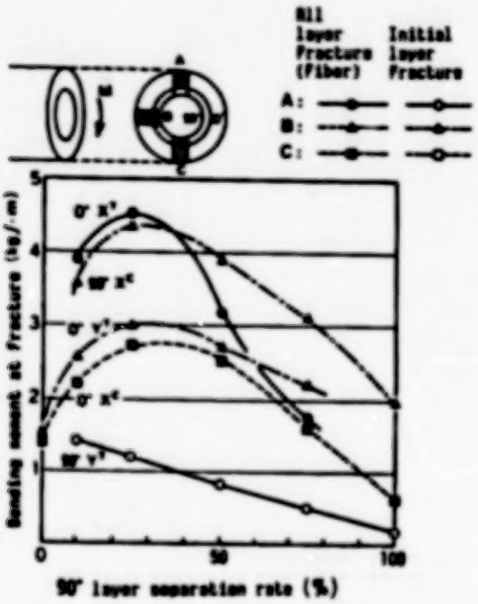

Figure 4. Flexural Strength of [0°/90°] Laminated Cylinder Tsai-Wu Canon Fracture Development Analysis

The relationship between the 90° layer separation rate and flexural strength in a [0°/90°] laminated cylinder in which a flexural load works is shown in Figure 4. The result of fracture progress analysis in various parts, such as the upper surface, lower surface, and side surfaces, showed that the initial layer fracture strength became minimum when the 90° layer separation rate was approximately 10 volume percent, and the entire layer of strength became minimum when the 90° layer separate rate was approximately 30 volume percent. The fracture of the cylinder is a 0° layer fiber compressive fracture in the compression part, and it is considered that a cylinder with a high flexural strength is available when an alumina fiber (ALF) with a high compressive strength has been hybrid laminated in the 0° direction.

The results of a case study on the laminating structure and flexural strength of the CF/ALF hybrid cylinder are provided in Figure 5. There was no strength improvement by the hybrid effect in this computation by the compounding rule, but the flexural strength was improved by more than 10 percent in the four-point flexural experiment. Furthermore, the peak load was approximately the same as that of a simple FRP substance in the Charpy impact test, but the impact value was improved by more than 40 percent.

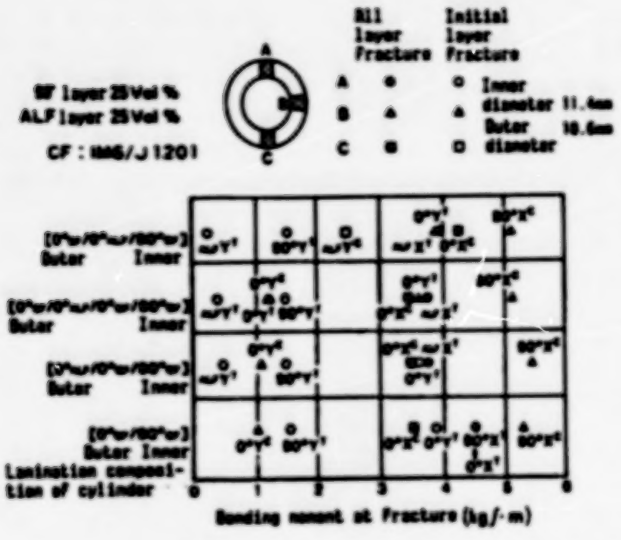

Figure 5. Lamination Structure of Cylinder and Bending Moment at Fracture

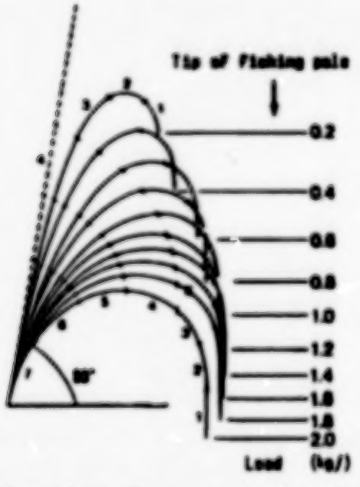

Figure 6. Deflection Curve and Load of Fishing Pole (Finite element method analysis)

The load-deflection curve of a fishing pole that was analyzed using the beam elements (14 elements) of the nonlinear finite element method "ABAQUS" is shown in Figure 6, and the comparison with the experiment is shown in Figure 7. The bending moment and axial tension of various fishing pole parts obtained by FEM computation in various stages of the lifting load were input in this software, and the fracture load of the various fishing pole parts obtained is shown in Figure 8. The No 3 fishing pole was fractured in the experiment under a load of 1.8 kgf. This means that the No 3 fishing pole was fractured at a lifting load of about 0.8 kgf in this analysis. The reason why the fracturing load is greater in the experiment than in the computation is considered to be due to the duplicated reinforcement effect of the various end parts of the fishing pole.

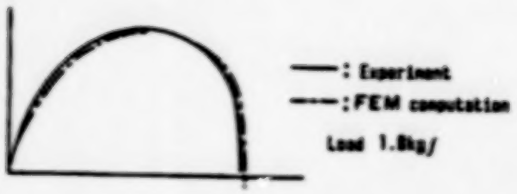

Figure 7. Comparison of Deflection Curve of Fishing Pole

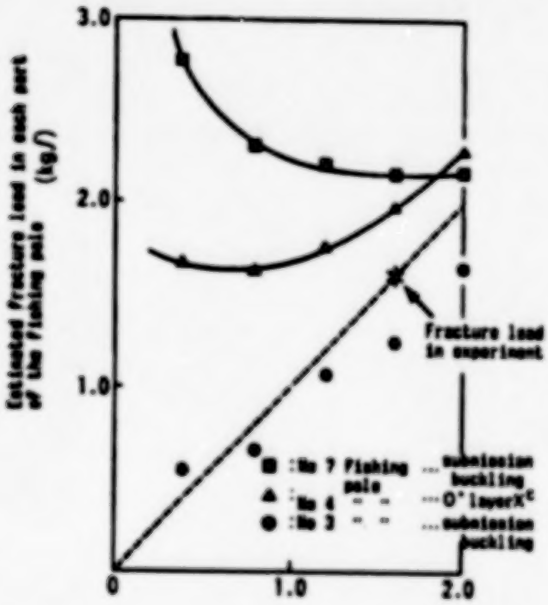

Figure 8. Lifting Load Used in FEM Computation (kgf)

4. Conclusion

(1) A software has been developed which performs stress-strain analysis, fracture progress analysis, and buckling analysis of each layer on a hybrid laminated cylinder, taking into consideration the compounding of loads and wet heat loads such as the axial direction tension/corrosion, torsion, bending, internal and external pressures, pulverization, etc.

(2) Using this software, it was possible to investigate the mechanism of fracture by bending, which had been difficult to estimate through experiment, by conducting a fracture progress analysis of the laminated cylinder that was subjected to a bending load.

(3) A cylinder of a CF/ALFRP hybrid laminated structure strong against bending could be developed by taking into consideration the flexural fracture mechanism of a laminatedcylinder.

(4) Great efforts and time were required for large deformation flexural analysis that took into consideration the flattening of the cylinder, but it was ascertained that such analyses could be promptly and accurately

performed by jointly using this software with finite element method analysis only.

References

1. J.M. Whitney and J.W. Gillespie, Jr., "CYLAN, Cylinder Analysis, Users Manual," August 1984, Center for Composite Materials, University of Delaware.

2. S.B. Dong, K.S. Pister, and R.L. Tailor, "On the Theory of Laminated Anisotropic Shells and Plates," J. THE AEROSPACE SCIENCE, Vol 29, 1962, University of California at Berkeley.

3. J.M. Whitney and J.C. Halpin, "Analysis of Laminated Anisotropic Tubes Under Combined Loading," J. COMPOSITE MATERIALS, Vol 2, No 3, 1968.

4. N.J. Pagano and J.M. Whitney, "Geometric Design of Composite Cylindrical Characterization Specimens," Ibid., Vol 4, July 1970.

5. A.A. Vicario and R.R. Rizza (Hercules Inc.), "Effect of Length on Laminated Thin Tubes Under Combined Loading," Ibid., April 1970.

6. N.J. Pagano, "Stress Gradients in Laminated Composite Cylinders," Ibid., Vol 15, April 1971.

7. J.M. Whitney, "On the Use of Shell Theory for Determining Stresses in Composite Cylinders," Ibid., Vol 5, July 1971.

8. Edited by Takeshi Hayashi, "Composite Material Engineering," Japan Science and Technology Federation, 1971.

9. D. Cohen and M.W. Hyer, "Residual Stress in Cross-Ply Composite Tubes," CCMS-84-04, VPI-E-84-16, Virginia Polytechnic Institute and State University.

10. Takeshi Hayashi, "On Buckling of Orthogonal Anisotropic Cylinder Shell," Shipbuilding Association Report, Report N 81, 1947.

11. NASA Space Vehicle Design Criteria (Structures), "Buckling of Thin-Walled Circular Cylinders," NASA-SP-8007, August 1968.

12. Edited by C.R.C. JAPAN, "Handbook of Structural Stability," CORONA Pub 1971.

20158/9365

Inspection of CFRP by Industrial X-Ray CT Scanner

43063807b Tokyo DAIJUNIKAI FUKUGO ZAIRYO SYMPOSIUM (KOEN YOSHISHU) in Japanese 22-23 Oct 87 pp 47-50

[Article from day 1, session 12, by Mineo Maruoka, Hideki Ohashi, and Masashi Fujii, Toshiba Corp.]

[Text] **1. Introduction**

X-ray fluorography and ultrasonic methods have been utilized as nondestructive methods to inspect CFRP structural parts. However, these methods have been insufficient for evaluating quantitatively the internal condition of three-dimensional shaped parts such as the CFRP joint and the pipe joint.

An industrial CT scanner capable of detecting the shape, internal defects, dimensions, etc., by nondestructive inspection was used in this research, and its application to CFRP parts was studied.

2. Investigation Items

(1) Evaluation of the possibility of void flaw detection by porous samples

(2) Evaluation of the fiber volume fraction (V_f) by the X-ray absorption coefficient (CT value)

(3) Inspection of CFRP bonded structural part

Figure 1. Appearance of CT Scanner

3. Outline of CT Scanner

The following are the main specifications of the CT scanner.

--Name	TOSCANER-3200 (Toshiba)
--Scanning system	Tested objective rotation system
--X-ray generation	140 kV, 300 mA
--Detector	High-voltage xe detector
--Image reconfiguration matrix	320 x 320 mm
--Picture element size	0.29 mm (photographing)
--CT value	-1,000 ~ 8,000
--Slice thickness	0.5, 2.5 mm
--Photographing range	150/24/300 mmϕ, 3-stage changeover
--Picture processing	Enlargement (X2), change of stage surface, profile display, histogram, zooming, scale display, image improvement processing

4. Specimens

(1) Disk sample (for pseudovoid and V_f evaluation)

--Shape	See Figure 2
--Molding material	Trayca T300 woven fabric (Toray Industries, Inc.) 250°F hardened epoxy
--Molding method	Hot pressing molding

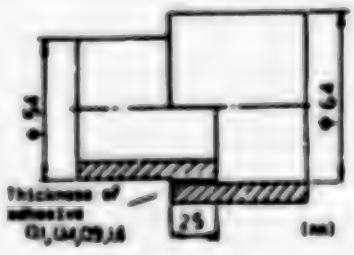

Figure 2. Disk-Shaped Sample

(2) Sample for evaluating the bonding condition

--Shape	See Figure 3
--Molding material	Trayca T300 roving (Toray Industries, Inc.) 250°C hardened epoxy
--Molding method	Filament winding molding
--Type of adhesives	Filler contained types, Al powder, $BaSO_4$, and SiO_2

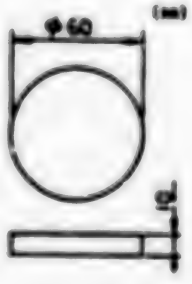

Figure 3. Sample for Adhesive Condition Evaluation

5. Results and Considerations

(1) Flaw detection and psuedovoids

Fault images of the CFRP sample with four types of holes opened (ϕ0.5, 1,0, 1.5, and 2 mm) are shown in Figure 4. The hole size (minimum 0.5 mm) and the CT value of the pseudovoid (air) can be read from the profile. The CT value is -1,000 (displayed as -150 due to gradation compression) and large when the void is large, and it shows the CT value of air. However, the size of a picture element constituting the fault image is 0.29 mm when the void is small, so the CT value of the surrounding CFRP is also taken in and an intermediate value between CFRP and air is shown.

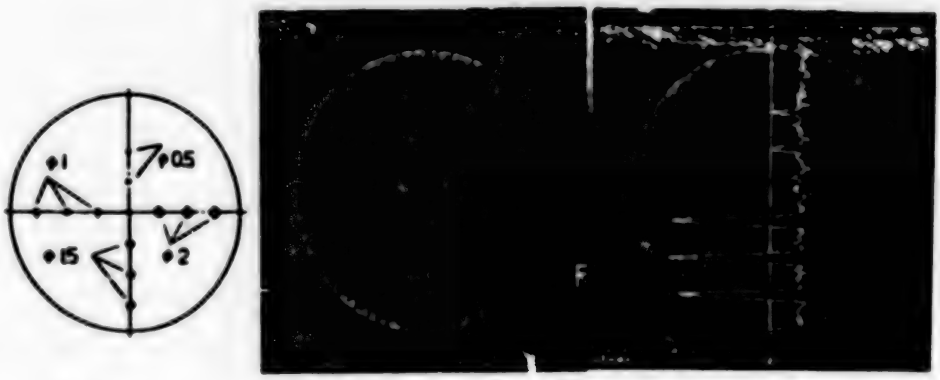

Figure 4. Void Flaw Detection by CT Scanner

(2) CT value evaluation of V_f

The evaluation results using disk samples wherein the V_f is changed are shown in Figures 5 and 6. The CT value changes from about 110 to 400 with the change of V_f in the case of voidless samples. In other words, V_f can be conversely estimated from the CT value. Since a portion of the resin is expelled and a void part is formed when molding is made with samples of 35 percent V_f and 45 percent V_f, the void part appears as a black dot. Since a void (air) effect is caused in this case, the CT value at the fault part shows a great dispersion and the apparent CT value of the entire CFRP is also subjected to this effect.

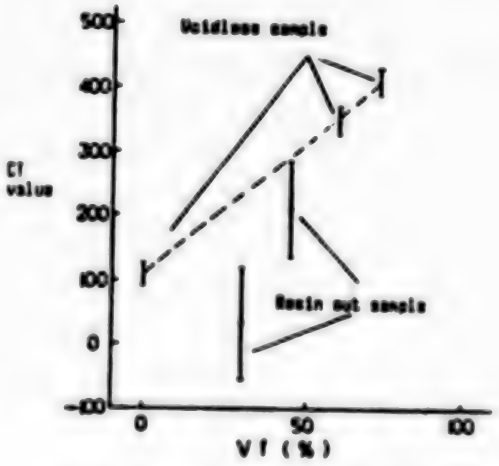

Figure 5. V_f and CT Value

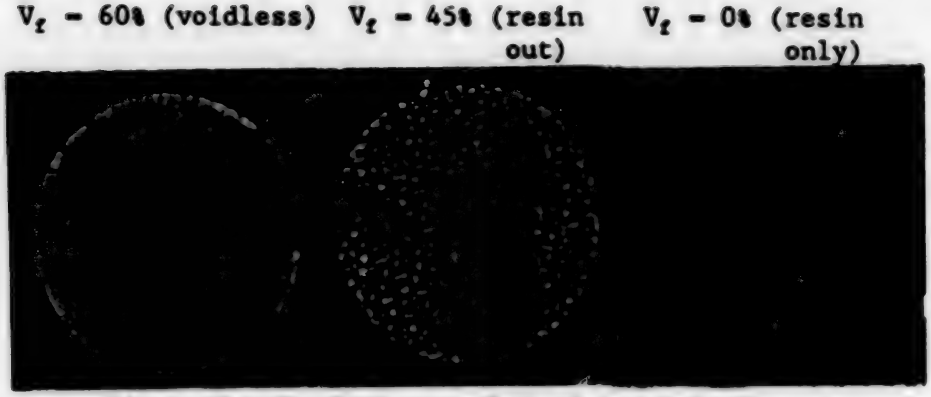

Figure 6. Fault Image of V_f Changed Samples

(3) Quantitative evaluation of bonded part

The CT value of adhesives changes greatly in accordance with the type of filler used, as shown in Table 1. The results of quantitative evaluation of the bonded part utilizing this characteristic are shown in Figures 7 and 8. The bonded part is shown by a white ring in samples with the CT value of the adhesive higher than that of CFRP. When the void part becomes a black dot and the T value becomes lower, it is possible to ascertain the abnormality of the charging amount and clearance of the adhesive by this CT value change. The bonded condition is clear when the bonded layer is thick, but distinguishability becomes limited when the thickness is about 0.1 mm (Figure 8). This is because the CT image is expressed in a form that also includes the CT value of the CFRP pipe when the adhesive thickness becomes smaller than a picture element (0.29 mm).

Table 1. CT Value of Adhesives

Type of adhesives	CT value	Type and volume of filler	
Adhesive A	1300	Al powder	60 percent
Adhesive B	8000	$BaSO_4$	45 percent
Adhesive C	120	SiO_2	20 percent
CFRP	2400		
CFRP	320	V_f · 60 percent	

Since the thickness for obtaining the highest adhesion strength is about 0.1 mm in structural adhesives, it can be said that the mixing of a heavy metallic salt such as $BaSO_4$ in the adhesive is effective as a means of facilitating nondestructive inspection by the CT scanner.

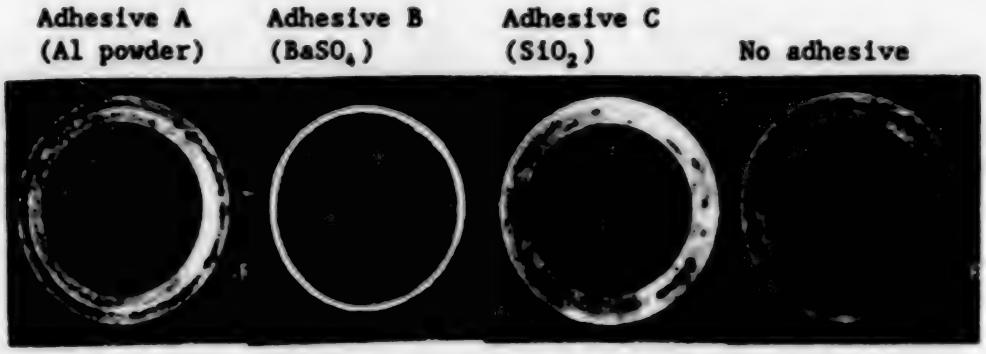

Figure 7. Fault Image of CFRP Adhesive Part

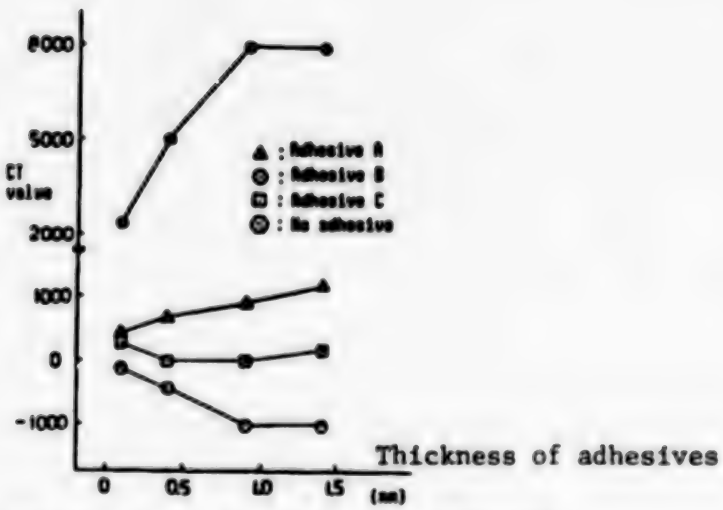

Figure 8. Thickness and CT Value of Adhesives

6. Inspection of Three-Dimensional Shaped Parts

An example of inspection of the CFRP joint developed for space structures is shown in Figure 9.

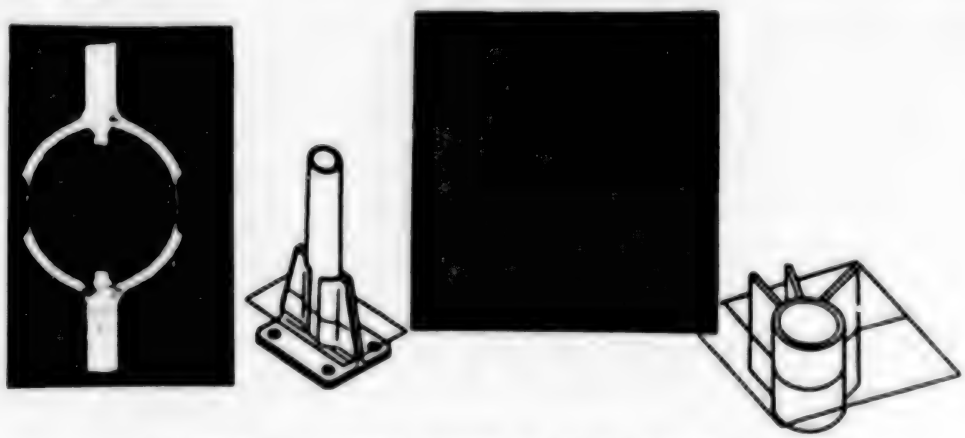

Figure 9. Fault Image of CFRP Joint

7. Conclusion

The CT scanner is able to evaluate quantitatively the internal condition of three-dimensional shaped parts, and its effectiveness has been confirmed sufficiently. A further minute evaluation and inspection will become possible in the future by improving the space resolution, realizing multichanneling and developing software exclusively for CFRP.

20158/9365

Simulation of Braiding of Three-Dimensional Composite

43063807c Tokyo DAIJUNIKAI FUKUGO ZAIRYO SYMPOSIUM (KOEN YOSHISHU) in Japanese 22-23 Oct 87 pp 87-90

[Article from day 1, session 21, by Atsushi Yokoyama, Osaka Prefectural Industrial Research Institute; Hidemitsu Kobayashi, graduate student of Kyoto Institute of Technology; and H. Hamada and Zenichiro Maekawa, Kyoto Institute of Technology]

[Text] **1. Introduction**

Textiles with a three-dimensional structure have attracted attention as reinforcing materials for composites, but for economic reasons, because a great deal of time and effort is required to produce these three-dimensional products, it can hardly be said that they are widely used today. In contrast, a braid structure is attracting attention as a reinforcing form for three-dimensional composites, as the basic mechanism of a braid structure is simple and the winding angle and textile structure can be changed by the initial conditions, such as spindle orientation, etc.

Therefore, in our research, a mechanism simulation program of a cord braid was prepared, and the simulation of various braid structures was conducted with the object of designing a braid structure by using a computer. A simulation method computing the initial condition in which a textile with a braiding angle set in advance was developed by controlling the braiding angle. An estimation of the critical braiding angle was made by considering carefully the fiber thickness. As one application, a simulation was conducted to obtain the conditions necessary for producing a braid with a uniform braiding angle on a special shaped cross-sectional cylinder in which the diameter was not fixed in the longitudinal direction. Also, studies were conducted on a new braiding structure aimed at producing a braid with complicated sections that differed from the conventional braiding structure.

2. Braid Structure

A braid is formed by guiding the motions of the fiber in two directions, horizontal and vertical. The motion in the horizontal direction is caused by the spindle, which is the holder of the bobbin, being moved and guided in the course, and the fiber coming out from the spindle is braided by the

spindles crossing each other alternately. The braided fiber is wound in the vertical direction by a take-up motion. the braid structures can be classified into two types: a flat braid structure and a cord braid structure. Diagrams of the spindle course and braid structure of the flat braid and cord braid are shown in Figures 1 and 2, respectively. The braid assumes a two-dimensional plate shape in a flat braid, and it assumes a three-dimensional hollow cylindrical shape in a cord braid. The latter cord braid was made the objective in this research.

Figure 1. Structure and Course of Flat Braid

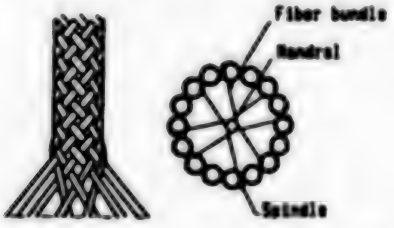

Figure 2. Structure and Course of Cord Braid

3. Braiding Mechanism Simulation of Cord Braid

3.1. Simulation method

The orientation angle of the fiber bundle braided against the longitudinal direction of the braiding cylinder was used for the braiding angle in this simulation. Among the various methods for setting the braiding angle, the method of setting the moving speed (revolving speed) of the spindle at a fixed rate and obtaining the prescribed braiding angle by changing the drawing-up speed of the mandrel that became the core of the produced braid was adopted in this simulation. A flow chart of the simulation program is shown in Figure 3. The following is the simulation method used. First of all, the revolving speed of the spindle, the initial position of the spindle and the braiding angle of the spindle are input as the initial conditions. Then, the braiding angle, revolving speed of the spindle, the drawing-up speed from the mandrel diameter and the coordinates of the fiber bundle on the mandrel are computed. The course of the fiber bundle is illustrated on the mandrel. It is judged whether or not the fiber bundle overlaps with the neighboring fiber bundle. The time change of the

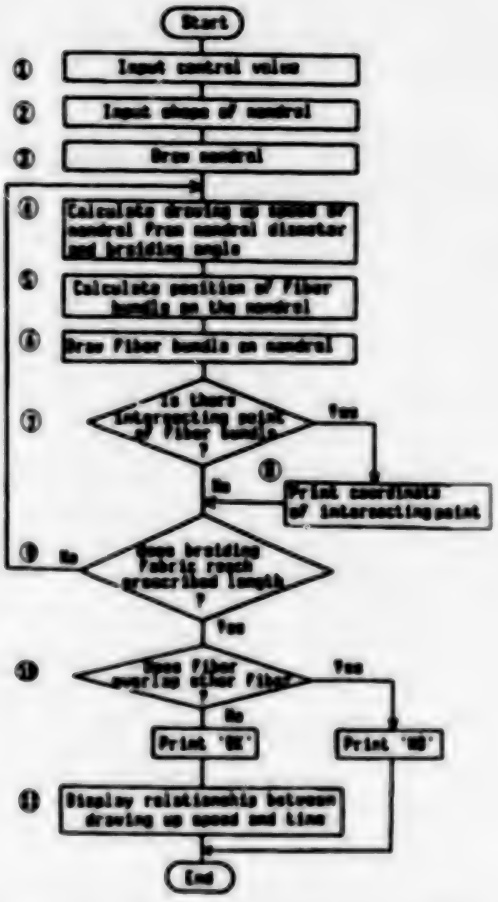

Figure 3. Flow Chart of Simulation Program

drawing-up speed is illustrated when the braiding fabric reaches its prescribed length, and this ends the simulation.

Next, a braiding was formed on the mandrel and a composite material cylinder was prepared by impregnating resin for studying the effectiveness of the simulation program. Carbon fiber and glass fiber were used as the fibers, and epoxy resin was used as the resin.

3.2. Simulation results

3.2.1. Braiding angle setting simulation

Three types of simulation results with difference drawing-up speeds are shown in Figure 4. the structure of the fiber is of a plain weave. For comparison, the appearance of a composite material cylinder prepared by actually using a carbon resin is shown. The structure of these resins shows a good conformity.

The fiber volume fraction of composite materials computed on the basis of the braiding angle and the simulation results computed by the simulation program are shown in Table 1. The fiber volume fraction becomes smaller as

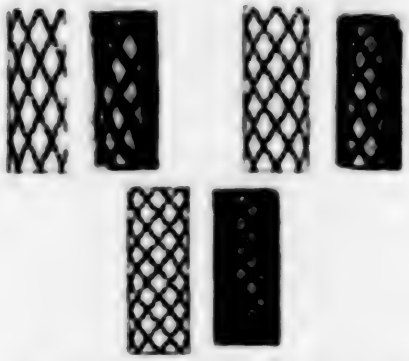

Figure 4. Simulation Results and Comparison of Composite Material Cylinders

Table 1. Braiding Angle and Fiber Volume Fraction of Composite Material Cylinders

Braiding angle (degree)	Experiment	26.0	34.0	42.5	56.8
	Simulation	25.8	32.5	42.5	60.7
Fiber volume fraction (%)	Experiment	49.3	46.7	43.6	48.0
	Simulation	47.4	44.8	39.9	41.3

the braiding angle becomes larger in braiding angles between 25.8° and 42.5°. This indicates the same trend as the actual measured values, and except for when the actual measure braiding angle is 56.8°, the braiding angle and fiber volume fraction coincide well.

Thus, it is clear that this simulation program expressed well the actual braid structure accuracy.

3.2.2. Critical braiding angle judging simulation

The possibility of preparing braidings in simulation by using various braiding angles is shown in Table 2. The result that the preparation of braiding was impossible was obtained when the braiding angle was 60.7°; the maximum braiding angle that was possible for preparation was 54.5°. This was the result obtained when a fiber bundle thickness of 4 mm, similar to that of glass fiber (microglass roving, number of fibers 1,600 each) was input, and this was because the fiber bundle overlapped with the neighboring fiber bundle when the braiding angle was more than 54.4°. Nor could a braiding be produced in the actual braiding process experiment conducted in this research when the braiding angle was 60.7°; the maximum braiding angle in which the braiding could be produced was 56.8°. This coincided approximately with the maximum braiding angle of 54.4° obtained by simulation, and thus it was clear that this program accurately expressed the actual limit of the braiding angle.

Table 2. Maximum Braiding Angle of Cord Braid

Braiding angle (degree)	25.8	32.5	42.5	60.7	Maximum braiding angle (degree)
Experiment	o	o	o	x	56.8
Simulation	o	o	o	x	54.4

3.2.3. Special shaped braiding cylinder simulation

Since the mandrel diameter changes in a special shaped cylinder wherein the diameter of the cylinder is not fixed in the longitudinal direction in the braiding process, the braiding angle changes greatly when braiding is conducted with the initial conditions unchanged. Therefore, it becomes necessary to gradually change the drawing-up speed of the mandrel when wishing to obtain a braiding with uniform braiding angle of a special shaped cylinder. The simulation result with the braiding angle fixed is shown in Figure 5. The graphs in Figure 5 show the changing condition of the mandrel drawing-up speed. A special shaped cylinder braiding with a fixed braiding angle can be produced by controlling the drawing-up speed of the mandrel in accordance with this simulation result.

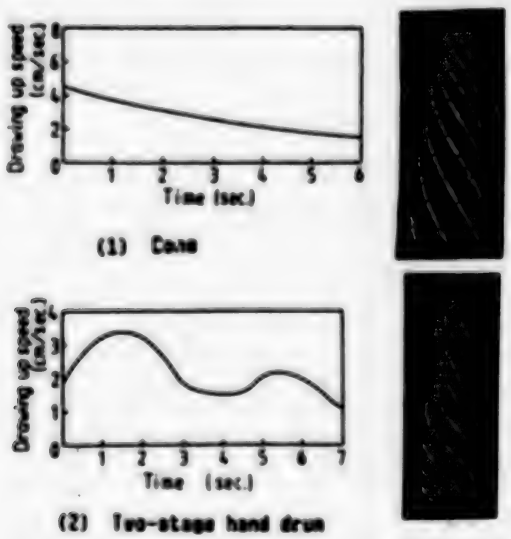

Figure 5. Simulation Results

4. New Braiding Mechanism

In conventional braiding machines, the speed of all spindles is fixed and the spindles are moved on a fixed course. The braidings that can be produced by this conventional mechanism are limited to only flat and cord braidings, not braidings with special shaped cross-sections, such as for example braidings having a concave type cross-section. Therefore, a braiding mechanism that travels independently on a plane course by

improving the mechanism was decided on, and the braiding simulation of a simple cord braiding by means of this new mechanism was conducted. In this simulation, the mechanism simulation program of cord braiding was modified, and the moving speed of various spindles instead of the drawing-up speed was changed so as to maintain the braiding angle in a fixed condition. The result of this simulation is shown in Figure 6. The relationship between the distance moved from the starting point and the drawing-up speed of the stainless steel is shown in Figure 7. As can be seen here, the complicated speed control of spindles is necessary even in such a simple cord braiding. The possibility of a braiding process by a new mechanism that moves each spindle independently was confirmed. Robotization is considered useful for the realization of this new braiding mechanism, and research on this is needed in the future.

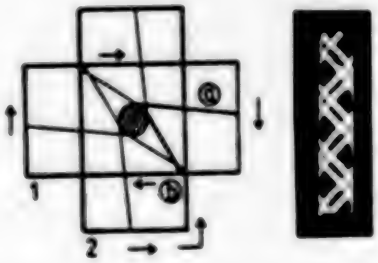

Figure 6. Simulation Result

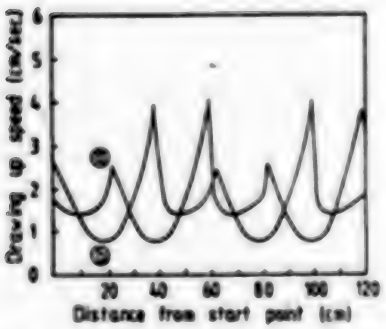

Figure 7. Speed Change of Spindle

5. Conclusion

(1) Computer simulation capable of estimating the structure of braiding by the spindle motion is possible.

(2) A simulation method computing the initial condition capable of producing a braiding cylinder with a prescribed braiding angle has been developed.

(3) Estimation of the braiding angle and fiber volume fraction of composite materials with a braiding structure is possible by means of this simulation program.

(4) It is clear that the computation of the braiding angle limit of braiding is possible.

(5) The drawing-up speed of the mandrel can be computed for producing special shaped cylinder braidings with a fixed braiding angle.

(6) A new mechanism for producing braiding with complicated cross-sectional shapes has been demonstrated.

Optimization of the braiding initial conditions has become possible by using this simulation program, and this can be considered as a useful means for supporting the designing of composite materials with a braiding structure.

We express our sincere thanks to Yasuhiko Iwasaki, graduate student of Kyoto Institute of Technology, for his considerable cooperation in preparing the simulation program for this research.

20158/9365

Continuous Forming of Carbon/Thermoplastics Composite Beams

43063807d Tokyo DAIJUNIKAI FUKUGO ZAIRYO SYMPOSIUM (KOEN YOSHISHU) in Japanese 22-23 Oct 87 pp 91-92

[Article from day 1, session 22, by Yoshiaki Sakatani, Yasuhiro Yamaguchi and Mikine Yoshida, Nagoya Aircraft Works, Mitsubishi Heavy Industries, Ltd.]

[Text] **1. Outline**

The continuous forming method of thin, long structural elements with a view to applications for future large-sized space structures is now being developed. Using a band plate shaped material of high elasticity type carbon fiber/PEEK, studies have been conducted on the basic processing conditions for passing it between rolls in stages and continuously forming it into a hat shape.

Optimum forming conditions such as the optimum forming temperature and optimum speed have been ascertained by gaining an understanding of formability data on materials from the forming tests conducted by the basic testing machines and from quality evaluation of the formed products.

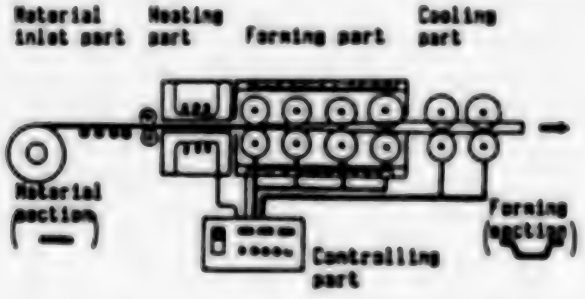

Figure 1. Basic Concept of Continuous Bending Forming

2. Objective

The objective of this research lies in the establishment of the following basic forming conditions for the continuous forming method of hot-shaped

cross-sectional thin, long structural elements by using carbon fiber thermoplastic resin.

(1) Gaining an understanding of formability data on forming materials.

(2) Optimization of forming conditions by trial manufacture tests.

3. Specimens

Table 1. Specimens

Material (Name of manufacturer)	Material composition		Lamination composition	Dimensions (mm)	Carbon fiber characteristics
	Reinforced fiber	Resin			
High elasticity carbon fiber/PEEK resin plate (Sumitomo Chemical Co. Ltd.)	High elastic modulus type carbon fiber (HM-CF) Vf: 60-70%	Polyether ketone (PEEK)	[0°] provided with ±45° glass cloth	1x150x150	No of Filaments: 12000 Density: 1830kg/m^3 Tensile strength: 1910 MPa Tensile elastic modulus: 343 GPa

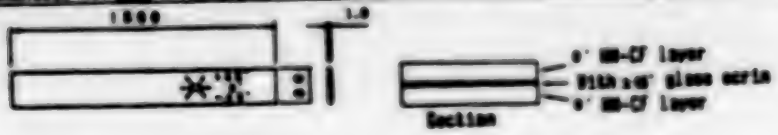

4. Basic Testing Machines

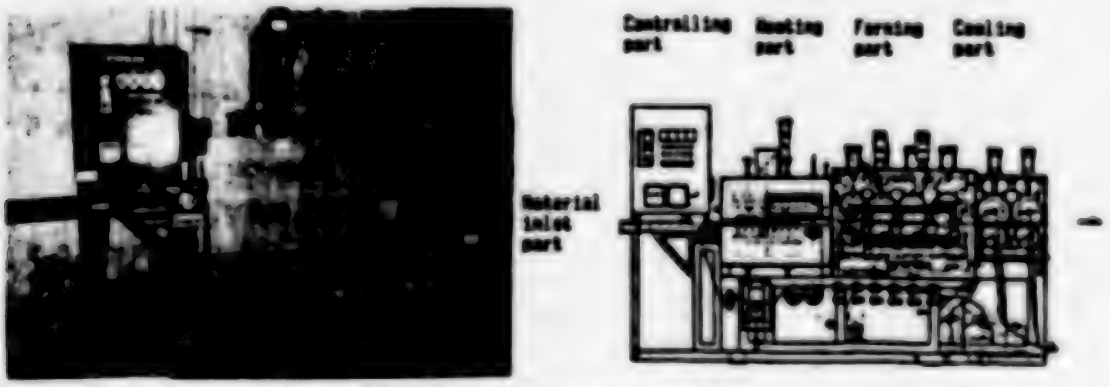

Figure 2. Basic Testing Machine

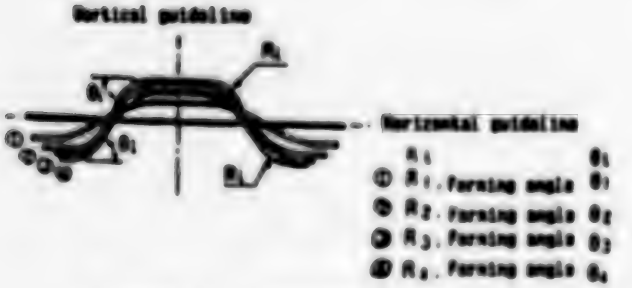

Figure 3. Forming Flower

5. Results

Table 2. Forming Conditions and Quality Evaluation Result of Formed Items

Case	Forming condition: Forming temperature K	Forming condition: * Forming roll angle θ_A/θ_B	Forming condition: * Cooling roll angle θ_A/θ_B	Forming rate m/h	Dimension accuracy Dispersion of plate %	Void rate Vol %	Tensile elastic modulus (GPa) (Dispersion rate)	** Forming angle θ
A	583	θ_1/θ_2	θ_3/θ_4	18	+3.3 -6.6	Max. 1.3	181 (+2.2 -0.5)	42- 58°
B	598	θ_5/θ_6	θ_7/θ_8	18	+1.9 -3.9	0.7 Max. 0.8	174 (+5.2 -4.0)	60- 62°

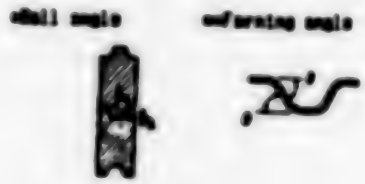

Figure 4. Appearance of Specimen After Forming Test (1500(L) x 66(W) x 17(H) mm)

6. Conclusion

This research was conducted as a link in the "Research and Development of Composite Materials" which was entrusted to the (Foundation) Association of Basic Technology for Future Metals and Composite Materials based on the Project of Basic Technology for Future Industries by the Agency of Industrial Science and Technology, MITI.

References

1. Sakaya, Manuscripts for First Basic Technology for Future Composite Materials Symposium, 1983, p 88.

2. Ibid., Manuscripts for Third Basic Technology for Future Composite Materials Symposium, 1985, p 17.

3. Ibid., Preliminary printing of 14th FRP Symposium, 1985, p 117.

20158/9365

Material Characterization of CF/AF Hybrid Fabric Laminates

43063807e Tokyo DAIJUNIKAI FUKUGO ZAIRYO SYMPOSIUM (KOEN YOSHISHU) in Japanese 22-23 Oct 87 pp 101-104

[Article from day 2, session 3, by Hideaki Kasano, Masataka Kawamura and Hiroyuki Matsumoto, Tokyo Institute of Technology]

[Text] **1. Introduction**

Since the hybrid fiber reinforced composite materials prepared by combining multiple fibers can be expected to improve the defects of single fiber reinforced composite materials, to manifest new characteristics and functions and to reduce costs,[1-3] research has been conventionally conducted on various hybrid composite materials that have suitably combined glass fiber, carbon fiber, aramid fiber, etc., and reports have been made on their basic characteristics and the synergistic effects of their hybridization. Moreover, separate works on hybrid composite materials[13] and detailed research reports on the material characteristics of GF/CF hybrid FRP laminates[14] have also been published, and it is believed that research in this field will become more and more active in the future. Against this background, in this research we have tried to evaluate the fracture toughness value from the viewpoint of fracture mechanics together with ascertaining the tensile and flexural elastic constants, fracture strain, fracture stress, etc., on CF/AF hybrid fabric laminates, on which research was previously limited to comparative research. These experimental results were compared with the results that could be estimated from the appropriate compounding rules and laminating theory, and studies were made of the various characteristics and special features brought about by the hybridization.

2. Preparation of Specimens

2.1. Component materials and forming method

The characteristics of the carbon fiber, aramid fiber, and epoxy resin used in this research and the specifications of the textile basic materials are shown in Table 1(a) and (b). The prepreg sheets were laminated according to laminated patterns that will be mentioned later, and the desired material boards were prepared by the autoclave forming method. The forming conditions were a temperature of 120°C, under pressure of 294 KPa, and the

Table 1.
(a) Characteristics of Fibers and Resin

	Carbon fiber	Aramid fiber	Epoxy resin
Name	T300-3000	Kepler-49	Toray Industries, Inc., #2500
Specific gravity	1.74	1.45	1.24
Tensile strength	3040 MPa	2765 MPa	3.96 GPa
Tensile elastic modulus	225.55 GPa	131.12 GPa	78 MPa
Tensile elongation	1.3 percent	2.4 percent	2.0 percent

(b) Specifications of Textile Basic Materials

Name	Toray Industries, Inc. Trayca cloth	Dupont Kepler cloth
Number	#6343	K-281
Braid	Flat braid	Flat braid
Density	5 /cm	6.8 cm
Weight	200 g/cm^2	178 g/cm^2
Thickness	0.27 mm/ply	0.285 mm/ply

pressurizing time was 1 hour. Then, short strip specimens 250 mm x 25 mm and 70 mm x 25 mm were cut out from these material boards for tensile and bending tests, and a tab was attached at both ends for the tensile test specimen. Also, for the fracture toughness test, a double-edge notched fracture toughness specimen was prepared by inserting an ideal fissure with a hacksaw and razor blade on both ends of a specimen with the same shape and size as that used in the case of a tensile test.

2.2. Laminated pattern

The hybrid types can be largely classified into a hybrid within strata type and a hybrid between strata type. Laminated patterns of CFRP and AFRP prepregs with the latter hybrid type as the objective were decided as follows. First of all, the plate thickness, made of the most basic laminated layer thickness, was set at about 1.25 mm after forming. The total number of laminated layers in this case becomes five layers, as the thickness of both types of prepreg sheets is about 0.25 mm. Moreover, the laminated patterns will be limited to eight types, taking into consideration the symmetry of the central surface, and only the six types

Table 2. Laminated Pattern (In the case of five layers)

No.	50	51	52	53	54	55
No 1 layer	A	A	A	C	C	C
No 2 layer	A	A	C	A	C	C
No 3 layer	A	C	A	C	A	C
No 4 layer	A	A	C	A	C	C
No 5 layer	A	A	A	C	C	C

A: AFRP C: CFRP

of laminated patterns listed in Table 2 were taken up after considering the time required for preparing the specimens from among these eight types of laminated patterns. It was necessary to further prepare two types of specimens with different plate thickness in order to ascertain the plate thickness effect in fracture toughness, and thus, laminated patterns of 10 and 15 layers were decided upon here, using the laminated patterns in the case of the five layers mentioned above as the basic model.

2.3. Mixing ratio of carbon resin

With the fiber volume fraction of the carbon fiber and aramid fiber V_fC and V_fA, respectively, the mixing ratio of carbon fiber against the total fiber volume fraction can be expressed as $V_fC/(V_fC + V_fA)$. The various characteristics of hybrid composite materials in this research have been arranged with this mixing ratio as the parameter. Now, since the fiber volume fraction of the carbon and aramid fibers of the CFRP and AFRP prepreg sheets is the same (60 percent) according to the specifications, it is considered that the total fiber volume fraction of laminates after forming and all fiber volume fractions of the carbon and aramid fiber of each layer are the same. Thereupon, the value of 0.506 (50.6 percent) was obtained in this research as a result of computing this value on the No 55 (CCCCC) specimen by the specific gravity method. On the other hand, the carbon fiber mixing ratio of hybrid composite materials is equivalent to the ratio of the number of laminated layers of the carbon prepreg sheets to the total number of laminated layers, based on the reason mentioned above. Therefore, the mixing ratio of carbon fiber in specimen Nos 50 to 55 in Table 2 becomes 0, 0.2, 04, 0.6, 0.8, and 1, respectively.

3. Experiment Method

The load-elongation was diagrammed together with measuring the load direction strain ϵ_x and the vertical direction strain ϵ_y by attaching an orthogonal gauge to both surfaces of a specimen in a tensile test. Also, uniaxial gauge was attached to a specimen in the longitudinal direction, and a four-point flexural test was conducted in a bending test. Furthermore, a tensile load was applied on three types of specimens with

different plate thicknesses by changing their respective crack length in four ways until the specimens were fractured, and the breaking load when fractured was read in the fracture toughness test. The tester used was the Instron TT-DM type tester and the load velocity was 2 mm/min in all cases.

4. Test Results and Considerations

4.1. Tensile Elastic Constant

Figure 1 provides a stress-strain diagram of the No 52 specimen as an example, and it was found that the stress-strain relationship of other specimens was also linear up to fracture. All elastic constants (E_x) in the tensile direction (X-axis direction) were obtained from the stress-strain diagram of each specimen. The tensile elastic constant of this fabric hybrid material was presumed as follows from analogy with the compounding rule[1] in the case of a unidirectional material by using the elastic constants E_fC and E_fA of the carbon and aramid fibers.

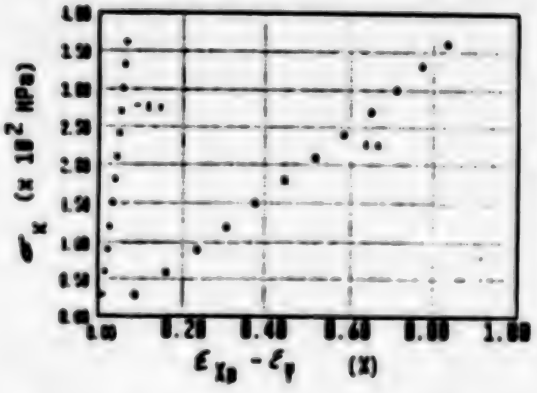

Figure 1. Stress-Strain Diagram
(Smooth tensile testpiece ACACA)

$$E_x = K_c E_f{}^C V_f{}^C + k_a E_f{}^A V_f{}^A \qquad (1)$$

Here, the correction coefficients K_c and K_a when $V_fA = 0$ and $V_fC = 0$, respectively,[1] were decided as $K_c = E/(E_fCV_fC) = 58.54/255.55/0.506 = 0.513$ and $K_a = E/(E_fAV_fA) = 33.11/131.14/0.506 = 0.499$ by using the test values of the Nos 55 and 50 specimens. On the other hand, the tensile elastic constant can be expressed as follows when applying the laminating theory.[14]

$$E_x = \sum_{i=1}^{n} K_i t_i - \frac{(\sum_{i=1}^{n} \nu_i K_i t_i)^2}{\sum_{i=1}^{n} K_i t_i}, \quad K_i = \frac{E_i}{1 - \nu_i^2} \qquad (2)$$

Here, n: total number of lamination layers; t_i, E_i, ν_i: plate thickness ratio and fiber direction elastic constant of the No i layer. The elastic constant of the carbon and aramid layers has been made the same as the elastic constant corresponding to the No 55 and No 50 laminate specimens.

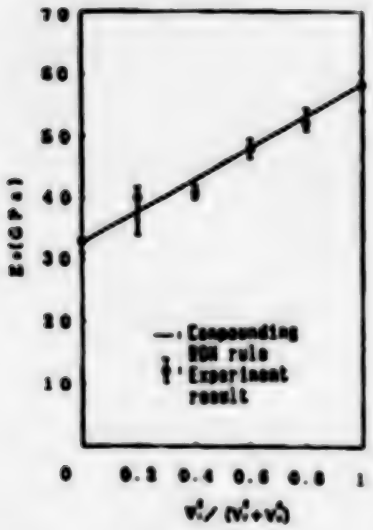

Figure 2. Effect of Rate of Carbon Fiber Volume Fraction Exerted on Tensile Elastic Constant

Table 3. Tensile Elastic Constant (Comparison between experiment results and computation results by the compounding (ROM) rule and lamination theory)

Laminated pattern	Experiment result	Compounding (ROM) rule	Lamination theory
AAAAA	33.11	33.11	33.11
AACAA	40.06	38.20	37.90
ACACA	40.92	43.28	40.92
CACAC	48.02	48.37	45.85
CCACC	52.11	53.46	51.62
CCCCC	58.54	58.54	58.54

(GPa)

these results are shown in Figure 2 and Table 3. The tensile elastic constant becomes greater as the mixing ratio of carbon fiber increases. It is clear that the dispersion of test values are small overall and they are close to values that can be estimated from the compounding rule and laminating theory.

4.2. Flexural Elastic Constant

The stress-strain relationship in the four-point flexural test is also approximately linear. However, the relationship becomes nonlinear as the aramid layers increase on the compressed side surface of laminates (Nos 50,

52, and 53 specimens) and as the strain becomes greater. It is believed that this is caused by the buckling behavior of aramid fibers on the compressed side surface. Figure 3 shows the relationship of the flexural elastic constant and the carbon fiber mixing ratio; there is a trend for the flexural elastic constant to become larger with an increase in the carbon fiber mixing ratio. Moreover, when comparing the test values with the values of the laminating theory, the test values are smaller by 5 to 14 percent where there is a carbon layer on the laminate surface side (Nos 53, 54, and 55 specimens). Furthermore, with the exception of the No 51 specimen case, the test values of the flexural elastic constant and the tensile elastic constant were approximately the same as the laminating theory values.

Figure 3. Effect of Rate of Carbon Fiber Volume Fraction Exerted on Bending Elastic Constant

4.3. Tensile Fracture Strain

Table 4 shows the fracture strain value (ϵ_g) of various specimens; although at one point the fracture strain of an aramid single fiber laminate (No 50 specimen) is about 1.8 times that of a carbon single fiber laminate (No 55 specimen), it is clear that the fracture strain of the aramid single fiber laminate decreases almost to the fracture strain of the carbon single fiber laminate. On the other hand, when studying in detail the example of the carbon single fiber laminate, we find that there is a trend for the fracture strain to increase slightly when the carbon layer is replaced by the aramid layer, and the effect of fracture strain increase becomes conspicuous when an aramid layer is especially arranged on the plate surface side and the carbon layers and aramid layers are laminated alternately (No 52 specimen). Figure 4 is a diagram that illustrates the results of Table 4.

4.4. Tensile Fracture Stress

Figure 5 shows the relationship between the tensile fracture stress σ_b and the carbon fiber mixing ratio. On the analogy that the stresses σ_{AFRP},

Table 4. Tensile Fracture Strain

Laminated pattern	Fracture strain (percent)
AAAAA	1.57
AACAA	0.97
ACACA	1.09
CACAC	0.91
CCACC	0.84
CCCCC	0.85

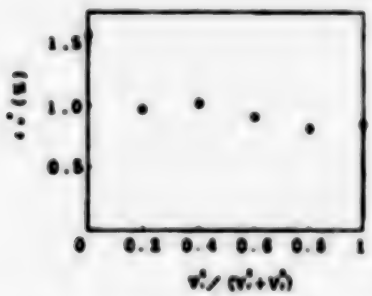

Figure 4. Effect of Rate of Carbon Fiber Volume Fraction Exerted on Tensile Fracture Strain

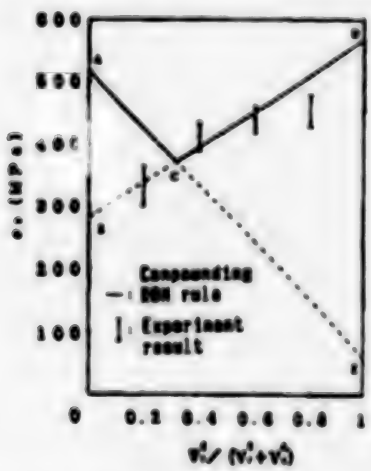

Figure 5. Effect of Rate of Carbon Fiber Volume Fraction Exerted on Tensile Fracture Stress

σ_{CFRP}, and σ_B of points A, D, and B in the diagram are those of a unidirectional material,[1] the tensile fracture stress can be expressed as follows by using the tensile strengths σ_t^C and σ_t^A of the carbon fiber and aramid layer.

$$\sigma_{AFRP} = k_A \sigma_t^A V_f^A, \quad \sigma_{CFRP} = k_c \sigma_t^C V_f^C$$
$$\sigma_B = K \sigma_{AFRP} \qquad (K = \epsilon_{CFRP}/\epsilon_{AFRP}) \tag{3}$$

Here, the correction coefficients k_A and k_C become $k_A = k_C = 0.369$ when using the maximum value of the tensile fracture stress of the Nos 50 and 55 specimens, respectively, as σ_{AFRP} and σ_{CFRP}.[3] Moreover, it becomes $K = 0.54$ when the tensile fracture strain is that of the Nos 50 and 55 specimens being used as the ϵ_{AFRP} and ϵ_{CFRP}. On the other hand, the stress of point E is expressed as $\sigma\epsilon = \sigma_m^2 (1 - V_f^A/^2)$. Here, σ_m^2 is the stress of the matrix resin when the aramid fiber breaks; however, the tensile strength of the matrix resin has been adopted in the case of this research based on the fact that the fracture strain of the aramid fiber and the matrix resin was about the same (2 percent). The tensile fracture stress suddenly drops at one point when the carbon layers are increased, but it becomes greater after this when the mixing ratio of carbon fibers is increased. Although there is a great dispersion in the test value compared with the case of the elastic constant, it qualitatively coincides with the trend that can be expected from the compounding rule.

4.5. Fracture Toughness

In this experiment, the stress-strain relationship up to fracture was almost linear, the development of cracks started simultaneously when reaching the maximum load (P_{max}), and fracture occurred almost in accordance with brittleness. Therefore, the fracture toughness K_c was computed by using the following evaluation formula by making σ_c the critical fracture stress (P_{max}/Wt) here.

$$K_c = \sigma_c \sqrt{\pi a F} \quad (2a/W)$$
$$F(\xi) = \frac{1.122 - 0.561\,\xi - 0.205\xi^2 + 0.471\,\xi^3 - 0.190\,\xi^4}{\sqrt{1 - \xi}}$$
$$(\xi = 2\,a/W) \tag{4}$$

Here, a is the crack length, W is the plate width, and t is the plate thickness of the DEN specimen. K_c was obtained for three types of specimens with different plate thicknesses by making crack length (a) 4 mm, 5.5 mm, 7.5 mm, and 9 mm. Figure 6 shows the relationship of K_c and the crack length on specimen No 53; it is clear that K_c is not dependent on the crack length and is almost fixed. This is also precisely the same for all the other specimens. Figures 7 and 8, respectively, show the relationship between K_c and the lamination layer thickness on the Nos 51 and 54 specimens. In contrast to K_c increasing as the lamination layer thickness is increased when there are more aramid layers than carbon layers, a reverse trend is seen when there are more carbon layers than aramid layers. Figure 9 shows the relationship of the K_c and carbon fiber mixing ratio in the case of five layers. The K_c value of hybrid laminates is small in comparison with that of carbon fiber simple laminates; it does not depend much on the mixing ratio of carbon fiber and is almost of the same degree.

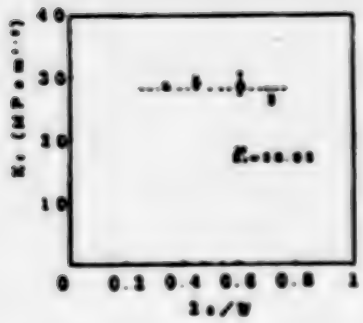

Figure 6. Effect of Crack Length Exerted on Fracture Toughness (DEN testpiece, CACAC, five layers)

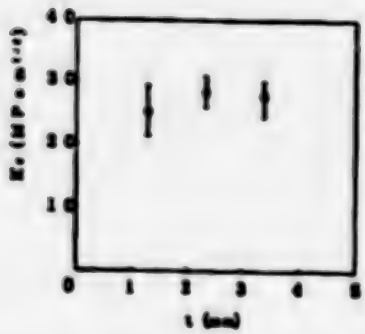

Figure 7. Effect of Testpiece Thickness Exerted on Fracture Toughness (DEN testpiece, AACAA)

Figure 8. Effect of Testpiece Thickness Exerted on Fracture Toughness (DEN testpiece, CCACC)

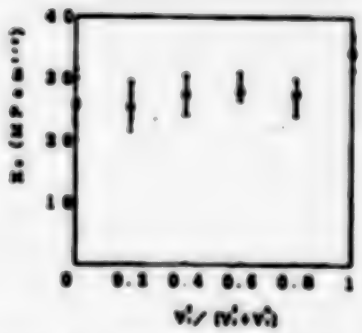

Figure 9. Effect of Rate of Carbon Fiber Volume Fraction Exerted on Fracture Toughness (DEN testpiece, five layers)

5. Conclusion

We were able to obtain various interesting data in this research, ascertaining mainly from an experimental viewpoint the basic material characteristics of carbon/aramid hybrid fabric laminates. As we did not make special reference to the synergistic effect of hybridization, this point remains to be explored as a future theme.

20158/9365

Compressive Strength of Fiber Reinforced Composite Materials

43063807f Tokyo DAIJUNIKAI FUKUGO ZAIRYO SYMPOSIUM (KOEN YOSHISHU) in Japanese 22-23 Oct 87 pp 125-128

[Article from day 2, session 9, by Akihito Kitano and Toshiaki Morita, Toray Industries, Inc.; and Kenichi Noguchi, Toray Research Center]

[Text] **1. Introduction**

Although suggestions have been made up to now on various aspects such as buckling, interface separation, and fiber fracture of many model fibers including those used in experiments, in regard to the shear buckling of a resin or composite material, the fracture mechanism has not necessarily been made clear.[1] The main reason for this is that the strength of the fiber itself cannot be measured in regard to compression, in contrast to the case of tension. Therefore, although it is certain that the aforementioned models and the factors of these models are concerned with the compressive strength of the fracture strain level of the fiber, it is not clear how and in what case. The compressive strength cannot be estimated so easily. And this complicates the discussion of factors such as the interface of fibers, resins, etc., from the standpoint of eliciting the latent strength of the fibers. Therefore, we have measured the compressive strength of composite materials comprised of various inorganic and organic fibers and have studied the relationship between the fiber characteristics and the compressive strength of composite materials. We have also measured the compressive strength of the fiber itself in various inorganic and organic fibers by means of the torsional elastic modulus and loop method related to the structural characteristics of fibers.

2. Experiment Method

The various inorganic and organic fibers that have been made the subject of this research are listed in Table 1. We mainly used the catalog values for the fiber tensile characteristic values in the table. These fibers can be large classified as carbon fibers, other inorganic fibers, and organic fibers. The carbon fibers were classified as PAN system carbon fibers and high elastic modulus Pitch system carbon fibers. The high-strength carbon fibers T800H, M40J, and M46J that have been newly developed in recent years were included among the PAN system carbon fibers, in addition to the conventional carbon fibers T300, M30, M40, and M46 of Toray Industries,

Table 1. Fibers Used in Experiment and Their Properties

Fiber		Filament diameter μ	Strength GPa	Modulus of elasticity GPa	Manufacturing companies
Carbon fiber PAN system "Trayca"	T300	6.9	3.53	230	Toray Industries, Inc.
	M30	6.3	3.92	294	"
	M40	6.5	2.74	392	"
	M46	6.4	2.35	451	"
	T800H	5.0	5.59	294	"
	M40J	5.2	4.40	392	"
	M46J	5.1	4.20	451	"
Pitch system "Carbonic"	HM60	10	2.70	620	Kashima Oil Co., Ltd.
Boron fiber "Boron Avco"	BF	100	3.50	410	Avco Corp.
Alumina fiber "Fiber FP"	AF	20	1.40	380	Du Pont Corp.
Glass fiber "RS57"	GF	13	3.00	74	Nitto Boseki Co., Ltd.
Aramid fiber "Kevlar"	KF	12	3.50	130	Du Pont Corp.
Polyethylene fiber "Spectra 900"	PF	38	2.60	120	Allied Chemical Corp.

Inc.[3] As shown in Table 1, the fiber tensile strength of the newer carbon fibers has been drastically improved in comparison with the conventional carbon fibers. In addition, boron fiber (BF), alumina fiber (AF), and glass fiber (GF) have been made the subjects of study of inorganic fibers, and the aramid fiber "Kevlar" (KF) and the high elastic modulus polyethylene fiber (PEF) have been made the subjects of study of organic fibers.

The compressive strength of fibers was obtained by the single fiber loop method,[4] as shown in Figure 1. That is, a loop was formed with a single fiber, the shape change being observed while tensioning the loop end and taking the strain when the ratio of the long axis/short axis increased more than the fixed value to be the compressive yield strain (E_fc) of the fiber. Then the compressive strength of the fiber itself was defined as $\sigma_fc = E_f \times \epsilon_fc$ by using this compressive yield strain value and hypothesizing that the compressive elastic modulus of the fiber was the same as the tensile elastic modulus of Table 1 also under a high compressive strain. The ratio of the long axis/short axis did not change; the fiber broke before indicating a yield in the glass fiber, boron fiber and alumina fiber; and the σ_fc (compressive strength of the fiber itself) was computed in this case by the means of the strain. Since it is considered that fracture probably occurred on the tensile side in these

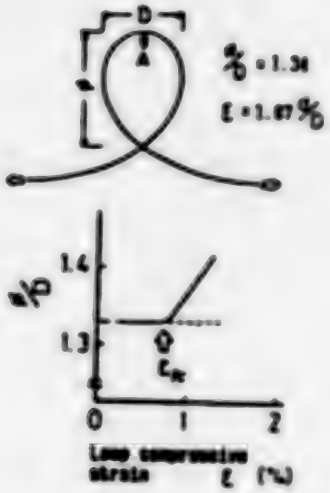

Figure 1. Loop Testing Method

fibers, it is considered that they have a higher fiber compressive strength. Moreover, the behavior in the case of fiber yield was observed by SEM on representative fibers. Computations were made on the aforementioned two measurements based on the premise that the fiber cross-section diameter is a true circle.

The epoxy resin No 3620 (180°C hardening type) made by Toray Industries, Inc. was used as one type of resin in the composite material in order to eliminate the resin factor. However, the #2500 (120°C hardening type) was used for the polyethylene fiber with a low melting point. (The resin modulus of elasticity for both epoxy resins is about 3.5 MPa.) This resin was used and a prepreg was prepared so that fiber volume fraction V_f became roughly 60 percent in a formed plate, and a unidirectional FRP plate was formed by an autoclave.

The compressive strength (σ_c) of the composite material was tested in conformity with the improved ASTM D695 by using the specimen shown in Figure 2. The compressive strength was converted into V_f = 60 percent. Moreover, a hybrid compressive sample--wherein a carbon fiber single layer was wrapped with a glass fiber layer--was prepared for observing the fracture behavior of resins in the composite materials for the PAN system carbon fibers T300, T800H, and M40. A strain equivalent to about 1.5 times the fracture strain of composite materials, in which each carbon fiber was independent, was applied, and the fracture behavior of the carbon fiber on the side surface of the polished sample was observed by optical microscope.

A three-point flexural test, simpler than the compressive test, was used to ascertain the latent high compressive strength possibility of CFRP. In addition to the ordinary test method, a measurement was made by inserting a cushion paper under the indenter[4] so as to ease the complicated stress generated in the neighborhood under the indenter. Also, a measurement under low temperature was made to ascertain the elastic modulus effect of resins.

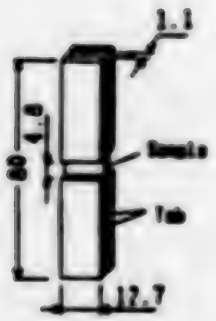

Figure 2. Compressive Testpiece Shape

3. Experiment Results

3.1.1. Outline of various fiber systems

The relationship between the composite material compressive strength and the anisotropic parameter (E_f/G_p) of the various fibers is shown in Figure 3. Apparently the anisotropy of the fiber produces an effect; the compressive strength as a composite material is low in fibers with large anisotropy (PEF< KF, Pitch system CF), and conversely, the compressive strength is high in fibers that are close to isotropy (BF< AF< CF). (It can be said that the compressive strength is high for CF when considering the fact that the modulus of elasticity is low in comparison to other fibers.) On the other hand, the PAN system carbon fibers among those studied have a medium-level anisotropy, and the compressive strength is also in an intermediate position.

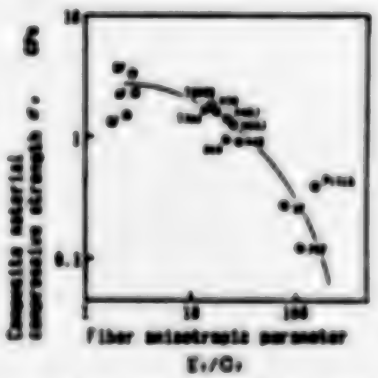

Figure 3. Relationship of σ_c and E_f/G_f

The relationship between the fiber compressive strength and the composite material compressive strength obtained by the loop method is shown in Figure 4. Although there is a simple discrepancy from the compounding rule, a good relationship, wherein the compressive strength of the composite materials is also low, is seen in fibers (PEF< KF< Pitch system CF, M40, M46) in which the compressive strength of the fiber itself is low. In other words, it is accurate to say that these fibers, rather than having

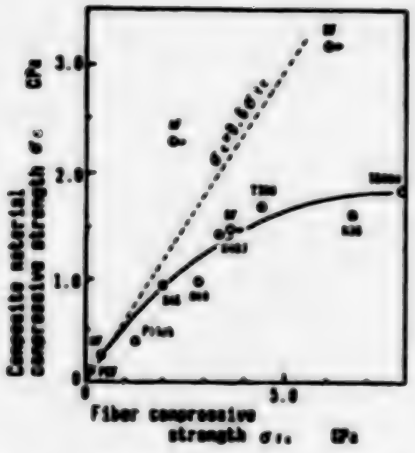

Figure 4. Correspondence of σ_c and σ_{fc}

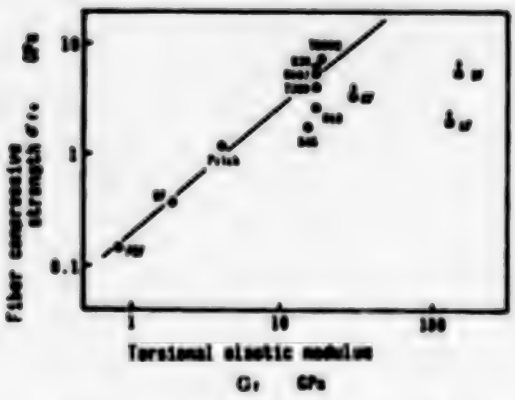

Figure 5. G_t Dependency of σ_c

large anisotropy in themselves, easily generate shear buckling as their torsional elastic modulus is low, as shown in Figure 5, and therefore the compressive strength of the fibers themselves is low. As already indicated, in KF[6] it can be considered that the low compressive strength of these fiber composite materials is caused by the low compressive strength of the fibers themselves. It has actually been observed by SEM that the fiber itself yielded on the compressive side and generated a "kink"[3,6] under the loop test in these fibers. (However, in the T300 and T800H fibers, such a yielding condition has not been observed as of today, as the fixation of specimens is difficult.) In PEF and Af used as a composite material, a yield fracture that did not divide the specimen into sections under compression appeared

In Pitch system carbon fibers, the compressive strength is low for the fiber itself or as a composite material, and it can be considered that this is also caused by the low torsional elastic modulus.

BF and AF, as mentioned above, show a high compressive strength as a composite material. It is now thought that the reason for this is because

the fibers are isotropic and have a high torsional elastic modulus--instead of the reason generally given in the past, that the fiber diameter is thick--and because they are considered to have an especially high fiber compressive strength on the basis of extrapolating the relationship shown in Figure 5.

(The effect of the fiber diameter is undeniable, but the reason for this may lie in the fact that it is advantageous in securing the straightness of a single fiber when forming composite materials rather than that it is a microbuckling of a simple single fiber. Fibers with extremely low G_f bend easily, and it is considered to be disadvantageous in strength manifestation also from this standpoint.)

3.2. Behavior of PAN System Carbon Fibers

In PAN system carbon fibers, it has been thought that the compressive strength of composite materials tends to decrease when the modulus of elasticity is high. The relationship between the fiber elastic modulus and the compressive strength of composite materials is shown in Figure 6. Now, while the compressive strength of composite materials decreases together with the increase in the modulus of elasticity, the compressive strength of the fiber itself has been improved in the new high-strength carbon fibers such as T800H, M40J, and M46JU, and the compressive strength has also been improved in comparison with conventional carbon fibers such as M30, M40, and M46. Moreover, in regard to the effect of the fiber diameter mentioned above, it is noteworthy that in comparison with the conventional carbon fibers, the new carbon fibers exhibit a high compressive strength as a composite material, despite the fact that the fiber diameter has become slender, as shown in Table 1. In other words, it is considered that the effect of the compressive strength improvement of the fiber itself is greater than the effect of the diameter in the manifestation of compressive strength of composite materials.

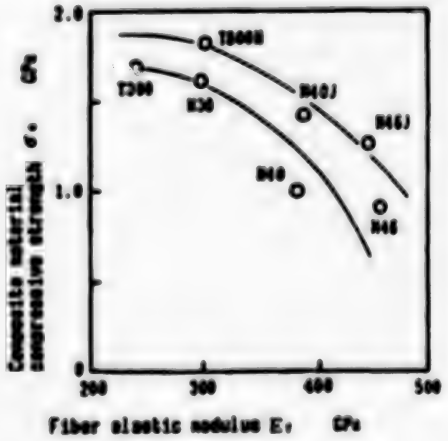

Figure 6. Relationship Between E_f and σ_c of CF

In regard to the reason for improvement of compressive strength of the fiber itself, however, there is no great difference from conventional

carbon fibers in regard to torsional elastic modulus, as shown in Figure 5. Therefore, it cannot be simply attributed to the structure of the fiber; it may be attributable to the decrease in defects reflected in the tensile strength improvement of fibers, as seen in Table 1.

The utilization factor of fiber compressive strength in composite materials tends to decrease as the fiber strength increases, as shown in Figure 4. However, it is thought that the reason for this is because a transfer is made to another control range with the improvement of strength from fiber control when the fiber strength is low. As a matter of fact, no fiber fracture was observed in the T300 and T800H carbon fibers even under a load strain greater than the fracture strain of the composite material of these fibers themselves, in contrast to the fiber fracture observed in the M40 carbon fiber, as shown in Figure 7, in the hybrid test wherein the carbon fiber single layer was enveloped in a glass fiber layer.

Figure 7. Fracture of M40CF in Composite Material
(Load strain ϵ = 0.8 percent)

In other words, while M40, M46, and pitch-based carbon fiber are in the fiber strength control range, T300 and M30, with a low elastic modulus range, are not.[7] Therefore, it can be considered that the improvement range of compressive strength for conventional carbon fibers in composite materials of M40J and M46J is greater than that of T800H carbon fiber, as shown in Figure 6. Conversely, this means that the latent high compressive strength of the fibers themselves, shown in Figures 4 and 5, has not been manifested in composite materials yet.

Although the latent high compressive strength of the T800H carbon fiber itself has not been demonstrated yet in a pure compressive crucible, as shown in Table 2, the strength is drastically improved in a bending crucible when the complicated shearing and bending stresses under the indenter are eased by the use of a cushion paper. Moreover, as shown in Figure 8, it has been confirmed that the bending strength at low temperature is drastically improved by reflecting the elastic modulus increase of the resin without using a cushion paper, and it is clear that the T800H carbon fiber showed a high compressive strength at least in the

Table 2. Flexural Strength When Using Cushion Paper

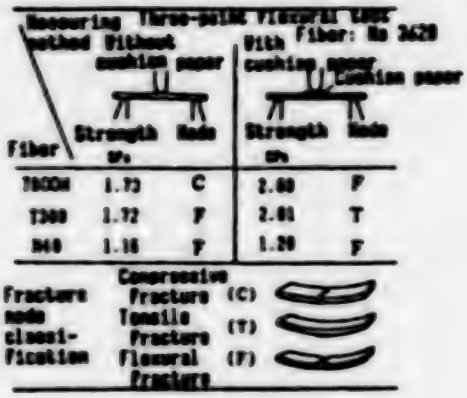

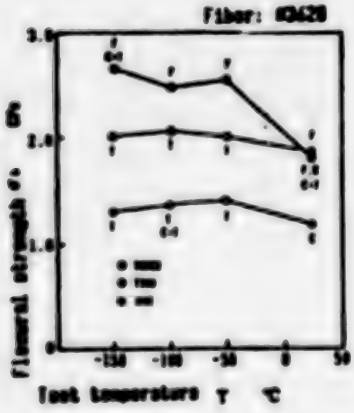

Figure 8. Flexural Strength Under Low Temperature Condition

bending crucible. (One of the reasons why the compressive strength of the T300 and M40 carbon fibers is not improved similar to that of the T800H carbon fiber is because the fracture generates on the tensile side and the tensile strength is in the rate-determining step, and it has been confirmed that the fracture strain (strength) is not improved at least in the M40 carbon fiber even when the T800H carbon fiber or glass fiber are arranged on the tensile side in order to prevent tensile fracture.)

This report has been undertaken from the standpoint of fiber compressive strength, but since the compressive strength of the fiber has a relationship with the G_f of the fiber, as shown in Figure 5, and the shearing elastic modulus of composite materials also has a relationship with the G_f, the compressive strength of a fiber can also be arranged according to the shearing elastic modulus of composite materials under the correlation of the compressive strength within the shear buckling of composite materials. A future topic of research will be quantitative handling, introducing the ineffective length concept in the compressive crucible, including the fiber buckling of the compressive crucible similar to the tensile crucible in regard to the discrepancy from the compounding rule, shown in Figure 4.

4. Conclusion

(1) The compressive strength of the fiber itself is low in fibers with a low torsional elastic modulus and large anisotropy (PEF<KF, and Pitch system CF), and therefore, the compressive strength of such composite materials is low. The high compressive strength of AF and BF composite materials is assumed to be due to the compressive strength of the fibers themselves being especially high, as these fibers are isotropic and their torsional elastic modulus is high.

(2) The compressive strength of the fiber itself obtained by the loop method corresponds well to the composite material compressive strength; the measurement made by the loop method is a powerful means to evaluate the compressive strength of the fiber itself.

(3) The tendency of the utilization factor to decline for the composite material compressive strength as the compressive strength of the fiber itself becomes higher is demonstrated in carbon fibers. It can be considered that the reason for this is because a transfer is made from the fiber strength control range to a range related to factors other than fiber. As a matter of fact, no carbon fiber fractures were observed in the T800H carbon fiber, in contrast to the carbon fiber fracture observed in the hybrid composite material of the M40 carbon fiber with low strength.

(4) In comparison with conventional carbon fiber, the high tensile strength carbon fiber developed in recent years, though having the same elastic modulus, shows a high compressive strength as a fiber and also as a composite material. Although a demonstration of the fiber latent high compressive strength has not been made in a pure compressive crucible for the T800H carbon fiber specifically, a high compressive strength was shown when a cushion paper was used and under low temperature in a bending crucible.

(5) Although shear buckling can be correlated to the shear elastic modulus of the fiber, resin or composite material apart from strength as the fracture mechanism, it can be considered as playing an important role in the manifestation of the compressive strength of composite materials. Shear buckling differs from Euler buckling, and cannot be prevented by shortening the specimen length.

References

1. D. Hull, "An Introduction to Composite Materials," Cambridge University Press, 1981.

2. S. Yamane, et al., 32d SAMPE, 1987, p 928.

3. Y. Sawada and A. Shindo, Extended Abstracts of International Symposium on Carbon, 1982, p 296.

4. W.R. Jones and J.W. Johnson, CARBON, Vol 9, 1971, p 645.

5. Onishi, et al., Preprinted Manuscripts of 10th FRP Symposium, 1981, p 5.

6. J.H. Greenwood and P.G. Rose, J. MATERIAL SCIENCE, Vol 9, 1974, p 1809.

7. H.T. Hahn and J.G. Williams, NASA TM 85834, 1984.

20158/9365

Testing of SiC Particle Reinforced Al Alloy

43063807g Tokyo DAIJUNIKAI FUKUGO ZAIRYO SYMPOSIUM (KOEN YOSHISHU) in Japanese 22-23 Oct 87 pp 149-152

[Article from day 2, session 14, by Toshiyasu Furuta, Furuta R&D Co., Ltd.; and Susumu Ushigome and Tomomi Soeda, Tokyo Yogyo Co., Ltd.]

[Text] 1. Introduction

Research and development is underway on many composite materials using metal as their matrix (MMC) and utilizing long fibers and whisker-shaped ceramics for reinforcing materials. However, the cost of these fibers and whiskers is still high, and high-level production technology is necessary for homogeneously dispersing these reinforcing materials.

In our research, we mixed SiC particles and A6061 atomized powder to produce round bar and plate-shaped Al alloys reinforced with SiC particles by means of hot extrusion. Sectional shapes such as round, tube, H, Z, T, etc., could be optionally selected by changing the die. This report will describe the characteristics (tension, high-temperature tension, compression, wear) that were obtained.

2. Extrusion Molding Method

A6061 alloy powder produced by the gas atomizing method was used in the matrix, and α type SiC particles were used for the reinforcing particles. The chemical composition of the matrix alloy and characteristics of the SiC particles are shown in Table 1. After dispersing and mixing the A6061 alloy powder and SiC particles, they were molded into billets and round bars of ϕ12 x 350 mm, and plates of 30 x 4 x 350 mm were molded by a hot extruder as samples. A flow chart of this extrusion molding method is shown in Figure 1.

3. Specimens

From these samples, various specimens were finished by machining. The shapes of the specimens are shown in Figures 2 to 5. T-6 treatment was used as the heat treatment.

Table 1. Chemical Composition of Matrix Alloy and Characteristics of Reinforcing Materials (Wet percent)

	Si	Fe	Cu	Mg	Mn	Cr	Zn	Al
A6061	0.76	0.51	0.28	0.96	0.04	0.21	0.10	Remainder

	Crystal system	Average particle diameter
SiC particle	α-type SiC	4.6 μm

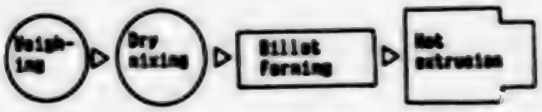

Figure 1. Powder Extrusion Molding Method

Figure 2. Tensile Testpiece

Figure 3. Compressive Testpiece

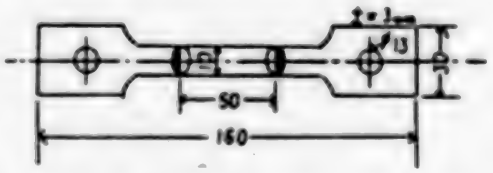

Figure 4. High-Temperature Tensile Testpiece

Figure 5. Abrasion Testpiece

4. Test Methods

4.1. Tensile test

An Instron type tensile tester (capacity 20 tons) was used as the tester, and strain measurement up to fracture was conducted by attaching two strain gauges (KFE-5-CL) to the central part of the specimen. The loading rate was 0.5 mm/second.

4.2. Compressive test

Strain gauges (KFE-5-CL and KRC-5-D17-11 L500) were attached to the side surface of the specimen; the former was used for measuring the strain up to fracture, and the latter for measuring the Poisson's ratio. When setting the specimen, a pressure sensitive paper was used at the upper and lower edge surfaces and adjusted so that a uniform load was placed on the specimen. The loading rate was 0.5 mm/second.

4.3. High-temperature tensile test

The chuck part was made in a ϕ13 perforated shaped, and a load was added via the pin. Since the elongation measurement of the parallel part was conducted in an electric furnace, two noncontact electronic optical system displacement measuring devices (Zimmer) were used, and the elongation of the upper and lower target gap of 50 mm was measured by using a differential amplifier. Moreover, a thermocouple (PR6462B/00) was fixed on the back side of the specimen using heat-resistant adhesive, and a test was conducted by applying a tensile load after the elapse of 10 minutes from the time the thermocouple indicated the set temperature. The test was conducted by an Instron type tensile tester (capacity 10 tons), and the loading rate was 0.5 mm/second.

4.4. Abrasion test

An Oogoshi type rapid abrasion tester was used for the abrasion test, and abrasion traces of the specimens mentioned above were measured by rotating the standard rotating disk (SKH3, H_RC90) and pressing it against the specimens at a fixed load.

5. Results

The result of the tensile elastic modulus is shown in Table 2 and that of the compressive elastic modulus in Table 3. The result of the tensile strength is shown in Table 4 and that of the compressive strength in Table 5. The result of the high-temperature tensile strength is shown in Figure 6 and the wear comparison result is shown in Figure 7.

Table 2. Tensile Elastic Modulus

Testpiece	Modulus of elasticity GPa	Average value GPa
6061	71.4-76.5	75.6
V_f - 20	108.8-113.1	111.3
V_f - 30	130.3-140.0	134.8

Table 3. Compressive Elastic Modulus

Testpiece	Modulus of elasticity GPa	Average value GPa
40L V_f- 0	71.2-72.9	72.2
40L V_f- 10	79.3-88.4	86.0
40L V_f- 20	96.5-104.9	101.0

Table 4. Tensile Strength

Testpiece	Tensile strength MPa	Average value MPa
6061	370 - 386	380
V_f - 20	410 - 433	423
V_f - 30	435 - 489	458

Table 5. Compressive Strength

Testpiece	Compressive strength MPa	Average value MPa
40L V_f- 0	407 - 452	425
40L V_f- 10	451 - 461	456
40L V_f- 20	452 - 470	461

Figure 6. High-Temperature Tensile Test of 6061Al and SiC/6061 With V_f of 20 Percent

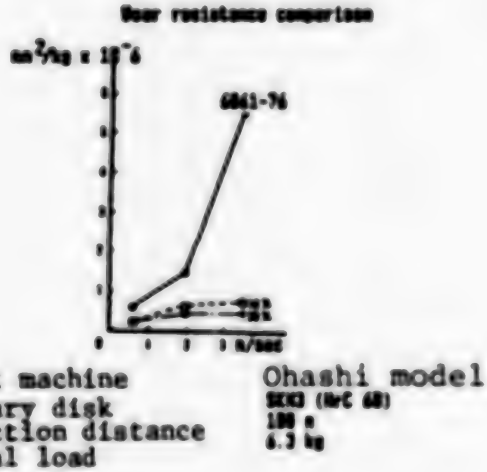

Figure 7. Comparison of Wear Resistance of 6061Al and SiC/6061 With V_f of 10 and 20 Percent

6. Considerations

A diagram of load-crosshead transfer when the V_f (volume fraction) of the SiC reinforcing particles is changed in the tensile test is shown in Figure 8. It is known that the relationship of strength and displacement is in inverse proportion. Photograph 1 shows the SEM result of the tensile fracture surface.

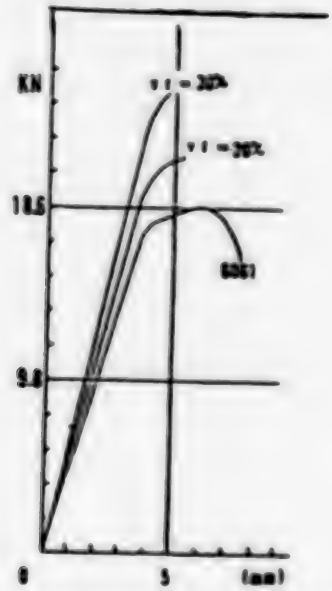

Figure 8. Diagram of Load-Crossheat Movement When V_f Is Changed

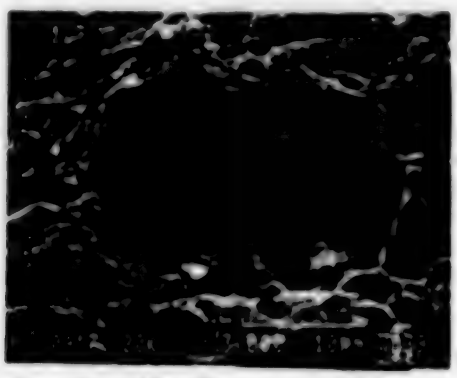

Photograph 1. Tensile Fracture Surface (X3000)

A diagram of the load-strain when the V_f of the SiC reinforcing particles is changed in the compressive test is shown in Figure 9. The inclination of the load changed in the neighborhood of 38.2 KN, and the V_f effect was not observed.

When comparing the V_f - 20 percent of SiC with the A6061 simple substance in the high-temperature tensile test, we found that at 200°C, the SiC V_f - 20 percent increased by 40 percent to 250 MPa, in comparison with 180 MPa for the A6061 simple substance.

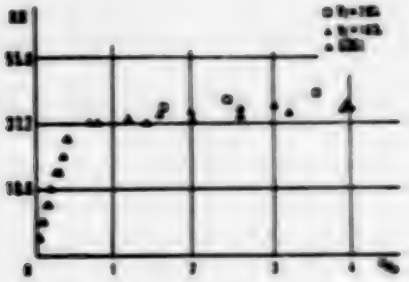

Figure 9. Diagram of Load-Strain When the Volume Fraction (V_f) Is Changed

When the V_f of SiC was changed in the abrasion test, the specific abrasion was practically fixed in the case of SiC V_f = 10 percent and SiC V_f = 20 percent, irrespective of the abrasion rate.

7. Conclusion

Although the tensile elastic modulus, tensile strength, and compressive elastic modulus increased together with the V_f increase of the reinforcing particle SiC, the compressive strength did not rise to the extent of the modulus of elasticity.

The high-temperature tensile test showed that it had a strength of 55 percent at a temperature of 200°C and a strength of 25 percent at 300°C compared with the room temperature strength.

In the abrasion test, the specific abrasion of SiC V_f = 10 percent was about 10 percent in 3.8 m/sec as compared with the A6061 simple substance.

In the future, a tensile fatigue test and an impact test will be examined.

We express our thanks to Koichi Ono, Yoichi Hayashi, Yoshio Aoki, and Masamichi Matsushima of the Fuselage Department of the National Aerospace Laboratory for their guidance on the test methods used in this research.

References

1. Furuta, et al., 22d Structure Strength Lecture, 100, 1980.

2. Matsushima, et al., 26th Structural Strength Lecture, 140, 1984.

3. Hayashi, et al., Ninth Composite Materials Symposium, 1984.

20158/9365

SiC Continuous Fiber Reinforced Aluminum Preform Wire

43063807h Tokyo DAIJUNIKAI FUKUGO ZAIRYO SYMPOSIUM (KOEN YOSHISHU) in Japanese 22-23 Oct 87 pp 157-160

[Article from day 2, session 16, by Yoshikazu Imai, Hiroshi Ichikawa, and Youichi Nagata, Nippon Carbide Co., Ltd., Laboratory]

[Text] **1. Objective**

In spite of the great expectations harbored for FRM (fiber reinforced metal), it can hardly be said that progress of its practical development is satisfactory. This is due to the fact that many problems had to be solved, and in particular to the fact that development of an effective FRM production method was delayed.

Therefore, the development of FRM was classified into "compounding" and "forming" production factors. The compounded basic materials were developed first of all, and these basic materials were made into FRM preforms. Then, the method of utilizing these preforms and making them into FRM formed products by various forming methods was adopted.

Specifically, the aim was to use the SiC continuous fiber "Nicalon" as the reinforcing material and to develop a compounded wire rod using Al as the matrix. This research was conducted as part of the Project of Basic Technology for Future Industries of MITI, and its target was the development of a long wire-shaped product with tensile strength of more than 1.47 GPa at room temperature and of more than 1.32 GPa at 450°C.

2. Method

SiC continuous fiber "Nicalon" (representative characteristics shown in Table 1) of a narrow-diameter multifilament was used for the reinforcing fiber, and pure Al and Al-system alloys were used for the matrix. In outline, the production method was a process to perform pretreatment such as removing the sizing agent of the fiber, passing the fiber through a matrix molten bath in a sufficiently open condition, and after impregnating and compounding the matrix thoroughly in the gaps of the multifilament, pulling out the fiber through the nozzle hole and conducting continuous winding.

Table 1. Representative Characteristics of Silicon Carbide Continuous Fiber "Nicalon"

Monofilament diameter	12.15 μm
Cross-sectional shape	Round shape
Number of filaments	250,500 each/yarn
Fineness	70,200 g/1,000
Density	2.55 g/cm^3
Tensile strength	2,500 to 3,000 MPa
Tensile elastic modulus	180 to 200 GPa
Maximum used temperature	1,250°C
Coefficient of thermal expansion	3.1 x 10^{-6}/°C

The mechanical strength of the prepared wire was evaluated by a tensile test, and the compounding condition was evaluated by the wire fracture, wire cross-section, and the appearance of the extracted fibers by using SEM.

The tensile strength at high temperature was evaluated by providing an infrared rapid heating furnace in the tensile tester. Various samples were measured after being maintained for 5 minutes at set temperature in air.

The fiber volume fraction (V_f) was obtained by melting the matrix with NaOH and computing on the basis of the extracted fiber weight.

3. Results and Considerations

3.1. Compounding condition

A cross-sectional SEM photograph of the prepared wire is shown in Figure 1, and a fracture SEM photograph after the tensile test is shown in Figure 2.

Figure 1. Cross-Section of Wire (SEM)

Despite the fact that the crowding of the fibers was fairly high, the osmosis of the matrix in the fiber gaps was sufficient; no parts that had not been impregnated by the matrix were seen in the fiber crowded parts. No dendrite-shaped voids, such as those sometimes generated through solidification and shrinkage of the matrix, were seen, either.

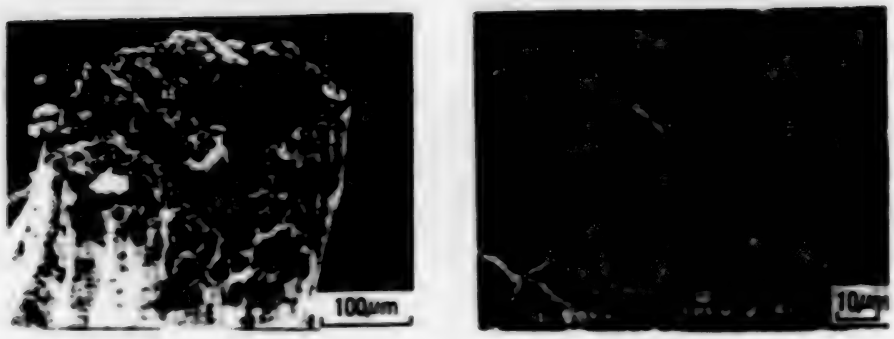

Figure 2. Fracture of Wire (SEM)

The unevenness was severe on the entire fracture, the pull-out of fibers from the matrix was moderately short, and superior wettability and adhesive property of the interface between the fiber and the matrix were exhibited. The fracture form of the matrix showed a large dimple pattern. On the other hand, the fracture form of the fiber showed a radial severe uneven surface such as is seen in high-strength FRM, and mirrors, mists, and hackles were observed.

Moreover, no changes before and after the compounding were observed in the extracted fibers. In short, it can be said from these observation results that the fibers presented an extremely sound compounding condition.

3.2. Tensile strength

The compounding rule (ROM, $\sigma_c = V_f\sigma_f + V_m\sigma_m$) is generally made the index for wire tensile strength, and the increase of V_f is effective for strength improvement. Therefore, a prototype was produced by gradually making the nozzle hole narrower and increasing the V_f by reducing the wire diameter. As can be seen from Figures 3 and 4, high characteristics by a high compounding rule ratio were realized when V_f was around 40 percent, but tensile strength broke away from ROM as the V_f became higher, and the strength improvement also tended to reach the uppermost limit. This was because infiltration fibers were drawn out through the small nozzle hole, and this was considered due to fiber damage caused by friction in the nozzle hole.

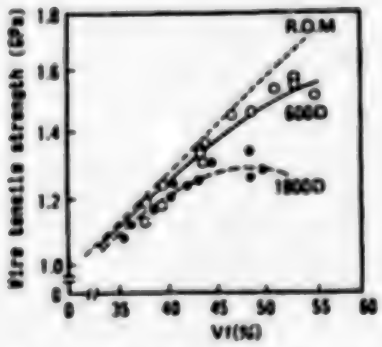

Figure 3. Fiber Volume Fraction (V_f) and Wire Tensile Strength

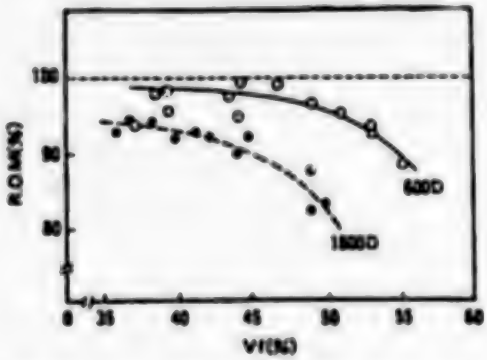

Figure 4. Fiber Volume Fraction (V_f) and ROM Percent

Therefore, a fiber with small kinkiness and with a better fiber straightness property was selected. Thus, a prototype was made whereby the 1800D (500 fil/yarn) fiber was replaced by a 600/d (250 fil/yarn) fiber. As a result, the ROM ratio was higher for the 600/d fiber than the 1800D fiber, a good wiring was possible up to a high V_f, and the tensile strength was improved.

Representative characteristics of the wire are provided in Table 2. The fiber V_f was 50 percent, the tensile strength was 150 GPa in a wire diameter of about 0.3 mmϕ, the strength utilization factor of the reinforcing fiber "Nicalon" was also high, about 90 percent, and the wire had a high strength. The Weibull modulus was high, 27 (Figure 5), indicating the high level of reliability of the material.

Table 2. Representative Characteristics of Nicalon/Al Preform Wire

Item	Characteristics	
Cross-sectional shape	Round shape	Round shape
Outer diameter	0.5 mm	0.3 mm
Fineness	500 g/1,000 m	170 g/1,000 m
Tensile strength	1,200 MPa	1,500 MPa
Tensile elastic modulus E_1 E_2	130 GPa 80 GPa	140 GPa 85 GPa
V_f	45 vol percent	50 vol percent
Minimum bending diameter	30 mm	20 mm

The high-temperature characteristics, as shown in Figure 6, were also superior; the tensile strength drop at high temperature was small even at a temperature of 450°C; the tensile strength was 1.35 GPa.

These results indicate that the target value of "Composite Materials (FRM)" under the Project of Basic Technology for Future Industries by MITI were met.

3.3. High-temperature tensile strength (450°C)

To study the approximately 10 percent strength drop at 450°C, upon following the same heat sequence as in the high-temperature tensile test, i.e., measuring the room temperature tensile strength after maintaining it for 5 minutes in a 450°C temperature there was no strength drop, as shown in Figure 7, and the initial room temperature was maintained.

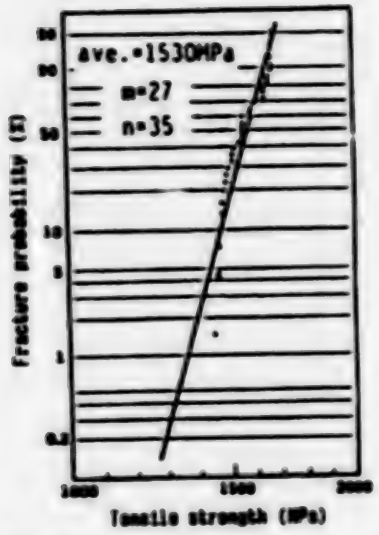

Figure 5. Weibull Distribution of Tensile Strength of Nicalon/Al Preform Wire
(Used the reliability analysis program by Assistant Professor Maekawa of the Kyoto Institute of Technology)

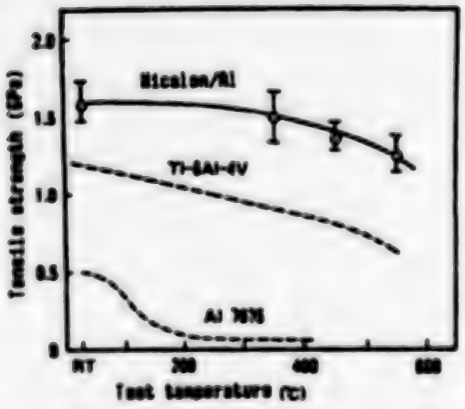

Figure 6. Result of High-Temperature Tensile Test of Wire

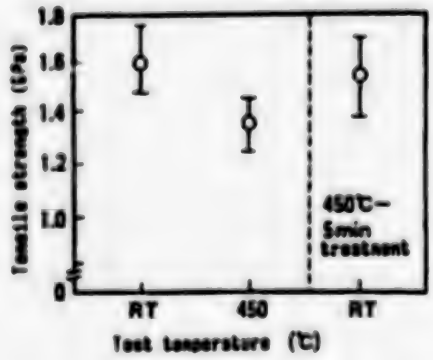

Figure 7. Wire Strength at Various Temperatures

The tensile fracture surface of these samples is shown in Figure 8. In the original high-temperature tensile test, the pull-out of fibers from the matrix is clearly longer in wire fracture (B) than in fracture (A), and a necking phenomenon is recognized.

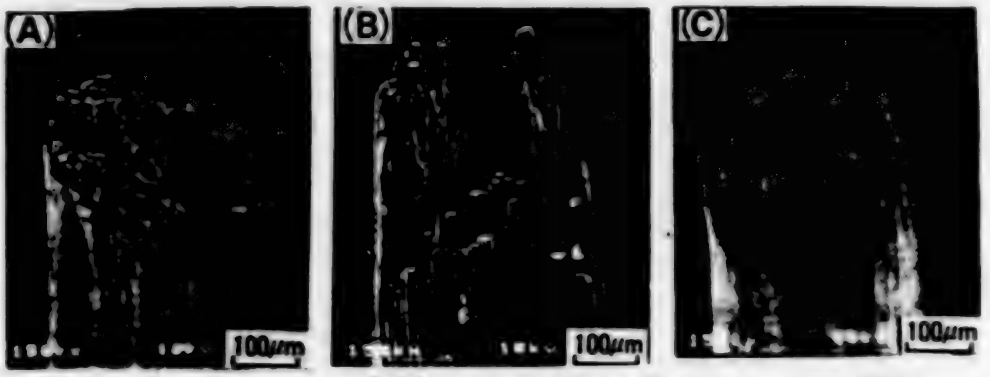

Figure 8. Fracture of Wire at Various Temperatures (SEM)

On the other hand, no practical difference was observed between wire fracture (C), measured on return to room temperature after undergoing the same heat sequence as in the high-temperature tensile test, and wire fracture (A), measured after the room-temperature tensile test. A strength of the same value as the room-temperature tensile strength was maintained.

No change was observed before and after the heat sequence in the strength and appearance of these extracted fibers.

It is considered on the basis of these results that the cause of the drop in wire strength at high temperature was not due to the drop in resin strength caused by the interface reaction, etc., at high temperature, but to the lowering of the stress propagation capacity of the fiber/matrix interface and the matrix caused by the softening of the matrix at high temperature.

Therefore, the Al-Al_3Ni system of directionally solidified eutectic was selected as the matrix in order to promote the thermal resistance of the matrix.

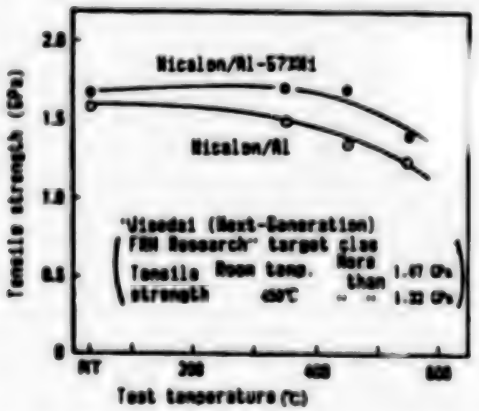

Figure 9. Result of High-Temperature Tensile Test of Wire

As a result, a Nicalon/Al system composite wire excelling in thermal resistance was obtained (Figure 9).

In the internal structure, an extremely fine fibrous or lamelliform eutectic phase of 0.01 to 1.0 μm was deposited in the matrix between fibers (Figure 10). This eutectic phase performed the work of plastic constraint at high temperature, and it is considered that the matrix thus also maintained a strength sufficient for stress propagation at high temperature.

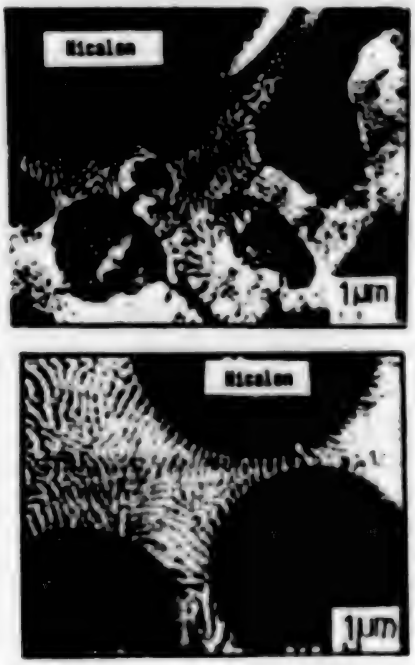

Figure 10. Internal Structure of Nicalon/Al-Ni System Wire (Fibrous and Lamella-shaped Eutectic Phase in Matrix)

Therefore, it can be said that this wire is a multireinforcing composite material for in-situ directionally solidified eutectic phase reinforcement and Nicalon long fiber reinforcement.

4. Conclusion

(1) A wire-shaped composite using SiC continuous fiber "Nicalon" as the reinforcing fiber and pure Al as the matrix was continuously produced by the infiltration method. The compounding condition of this composite was extremely sound, and the tensile strength also generally increased in parallel with the increase of V_f. The wire length was about 300 m, and the wire diameter was 0.3 mmϕ or 0.5 mmϕ.

(2) The high-strength wire had a fiber volume fraction (V_f) of 50 percent, a tensile strength of 1.50 GPa, a high Weibull modulus (27), and a high reliability. The high-temperature tensile strength at 450°C was 1.35 GPa, and at room temperature 90 percent of the tensile strength was maintained.

These values meet the "Target Values of Composite Materials (FRM) under the Project of Basic Technology for Future Industries" of MITI.

(3) It is considered that the cause of the drop in strength at high temperature was not the deterioration of the fibers, but the high-temperature characteristic behavior of the matrix. An in-situ directionally solidified eutectic system was adopted for improving the thermal resistance of the matrix, and a composite wire free from a drop in strength at 450°C was trial manufactured.

The trial produced wire was Al-5.79%Ni, the fiber V_f was 50 percent, and the tensile strength at both room temperature and high temperature was about 1.65 GPa. The matrix structure of this system showed a fine fibrous or lamelliform eutectic structure.

It is considered based on these facts that the Nicalon Al system composite wire is a promising practical material as an intermediate material (preform) for producing a high-performance FRM.

5. Supplementary Note

This research was conducted as part of the "Research and Development of Composite Materials" which was entrusted to the (Foundation) Association of Basic Technology for Future Metals and Composite Materials based on the Project of Basic Technology for Future Industries by the Agency of Industrial Science and Technology, MITI.

References

1. Yoshiro Minoda, Development of Jisedai Research MMC, Third U.S.-Japan Composite Material Society Meeting, 1986, p 475.

2. Kayama, Igata, Imai, Teranishi, and Ishikawa, Proc. ICCM-V, 1985, p 609.

3. Ishikawa, Proc. IUPAC CHEMRAWN-VI, T-21, 1987.

4. Ishikawa, Yamazoe, and Imai, Ibid., IIF04, 1987.

5. Imai, Manuscripts of Second Jisedai Composite Material Symposium, 1984, p 121.

20158/9365

Hot-Press Forming of Multifilament Fiber Reinforced Metals

430638071 Tokyo DAIJUNIKAI FUKUGO ZAIRYO SYMPOSIUM (KOEN YOSHISHU) in Japanese 22-23 Oct 87 pp 161-164

[Article from day 2, session 17, by Akira Sakamoto and Chikara Fujiwara, Mitsubishi Heavy Industries, Ltd., Nagoya Aircraft Works]

[Text] 1. Outline

A hybrid material comprised of 0°/90° angle ply material and titanium alloy was formed for the purpose of improving the 90° direction strength (90° strength) against the fiber direction, together with studying the hot pressing process on the material system of C/Al, SiC(pcs)/Al and SiC(CVD)/Al. The mechanical characteristics of these compacts were studied and evaluated.

2. Forming Process

If compounding can be achieved in a good condition, a lower forming temperature of the preform is desired in the forming of FRM from the standpoint of controlling the reaction of the fiber/matrix interface. Therefore, an Al alloy sheet with a solid phase temperature lower than the matrix metal of the wire preform was inserted between the wire preform lamination layers of SiC(pcs)/Al and C/Al developed by the raw materials group of the Association of Basic Technology for Future Metals and Composite Materials, and a sheet insert was developed for mutually improving the bonding property of the wire preforms. As a result, the mechanical characteristics of the compacts were improved. Although the mutual bonding of the M40/5056 wire preforms is insufficient in the forming conditions of 803 K x 30 min x 39.2 MPa, superior compounding is available under the same forming conditions with a sheet insertion (Figures 1 and 2). The strength of SiC(pcs)/1050 compacts using the insert method are shown in Table 1. The 90° strength is high (97 MPa) without detracting from the 0° strength achieved by the 2017 insert, and it can be considered that the bonding of the wire preforms is superior. On the other hand, bonding is insufficient using the 4343 insert (Figure 3), and the 90° strength is of a low value. The lower the solid phase temperature of the Al alloy, the more effective it will be as an insert material.

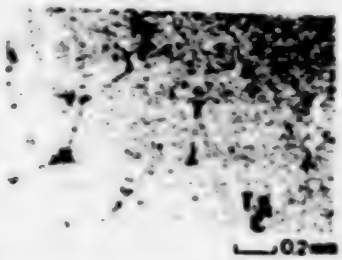

Figure 1. Microstructure of M40/5056 Compact
(Forming conditions 823 K, 30 min, 39.2 MPa)

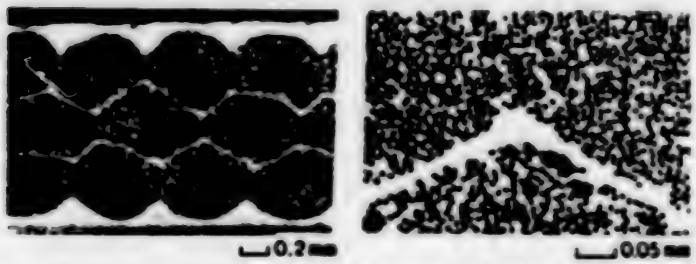

Figure 2. Microstructure of M40/5056 + 2017 Sheet Insert Compact
(Forming conditions 803 K, 30 min., 39.2 MPa)

Table 1. Forming Conditions of SiC(pcs)/1050 by Sheet Insert Method and Tensile Test Results

Preform	Forming conditions: Method	T_1 / T_2 (K)	t_1/t_2 (min)	P (MPa)	V_f (%)	Density (Mg/m³)	Tensile strength 0° Aver. Min. Max. (MPa)	Tensile strength 90° Aver. Min. Max. (MPa)	Modulus of elasticity 0° Aver. Min. Max. (GPa)	Elongation 0° Aver. Min. Max. (%)
SiC (pcs)/ 1050 +4343	Hot platen	803	30	39.2	36	2.7	837 798 906 (6)	35 32 38 (2)	115 111 125 (6)	>1.07 1.06 >1.07 (6)
SiC (pcs)/ 1050 +2017		803	30	39.2	36	2.7	846 775 909 (10)	97 83 110 (2)	110 108 112 (2)	>1.07 >1.07 >1.07 (2)

( ) Figures in parentheses indicate number of samples.

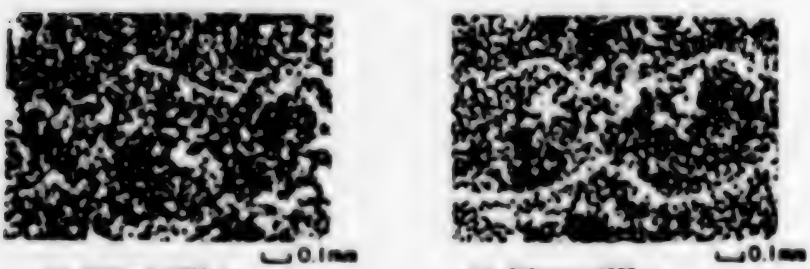

(a) SiC(pcs)/1050 + 4343 sheet insert compact

(b) SiC(pcs)/1050 + 2017 sheet insert compact

Figure 3. Microstructure of SiC(pcs)/Al Compact

3. 0°/90° Angle Ply Material

The 0°/90° angle ply materials comprised of M30/5056, SiC(pcs)/1050, and SiC(CVD)/6061 (Figure 4) were formed, and the azimuthal dependency of the tensile characteristic (Figure 5) of these compacts was obtained. A great directional dependency could be ascertained in the tensile strength. The 0° strength was about one-half that of unidirectional reinforced material, and the 15° strength was greatly diminished. Almost no changes were observed from 15° to 45° in the C/Al system and the SiC(pcs)/Al, whereas the dropping of strength continued up to 45° in the SiC(CVD)/Al. The strength was the lowest at 45° in the 0°/90° angle ply materials, and this was some two to three times the 90° strength, which represents the lowest strength in a unidirectional reinforced material for all systems. An azimuthal dependency was also recognized in the modulus of elasticity, but it was not as great as the strength. The tensile fracture surface is shown in Figure 6.

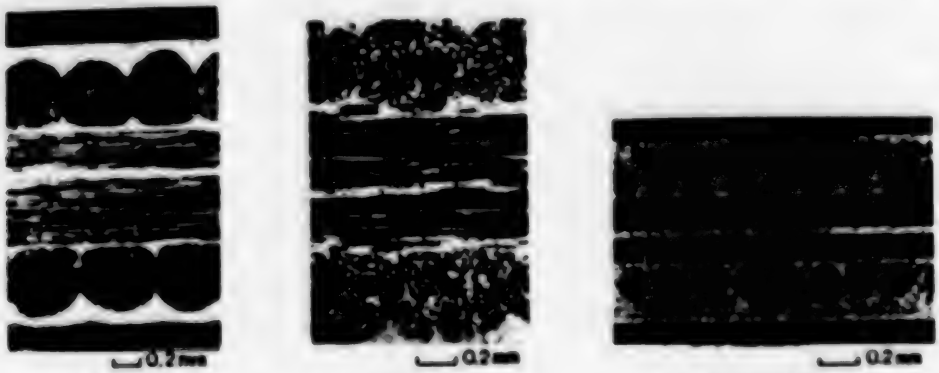

(a) M30/5056 (b) SiC(pcs)/1050 (c) SiC(CVD)/6061

Figure 4. Sectional Microstructure of 0°/90° Angle Ply Material

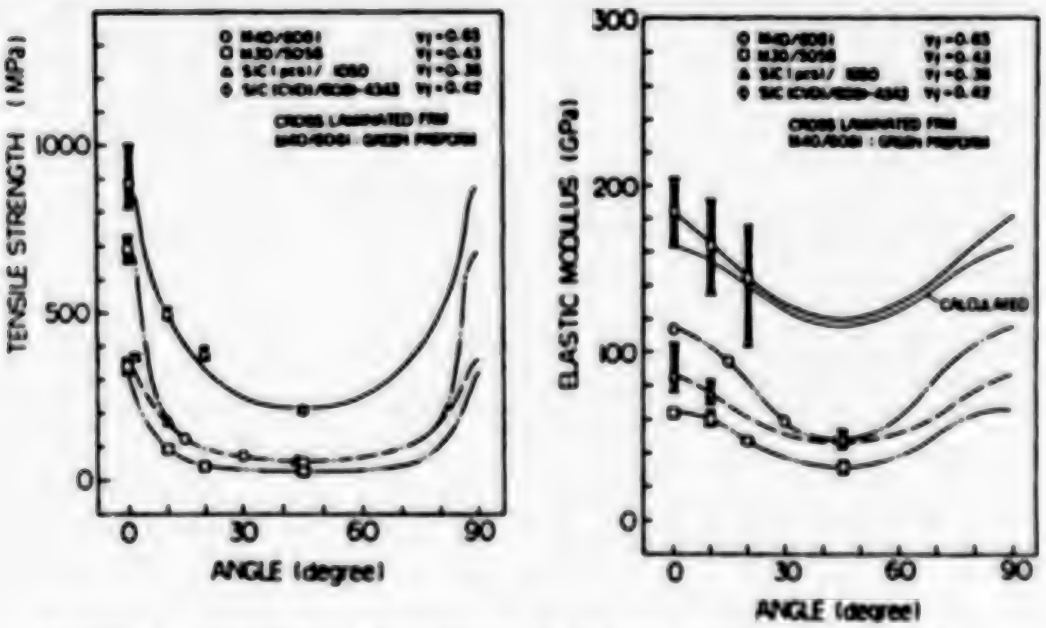

Figure 5. Azimuthal Dependency of 0°/90° Angle Ply Material

(a) M30/5056(45° tension) (b) SiC(pcs)/1050(0° tension) (c) SiC(CVD)/6061(0° tension)

Figure 6. Fracture Shape of 0°/90° Angle Ply Material

The anisotropy is still great in the angle ply material, and it can be said that the weakest azimuthal strength (45° strength) is still comparatively low.

4. Hybrid Materials

A hybrid material of Al matrix composite material and Ti alloy was formed. The cross sectional microstructure is shown in Figure 7. The compounding was superior, and the bonding of the Al alloy and Ti alloy was also superior. The results of a tensile test are arranged in Table 2, together with the forming conditions. The 90° strength of hybrid materials M30/5056 + Ti-3Al-2.5V and SiC(pcs)/1050 + Ti-3Al-2.5V was 151 MPa and 186 MPa, respectively, a drastic improvement to some five to eight times that of FRM compacts. The tensile fracture of these hybrid materials is shown in Figure 8. It can be confirmed that the bonding of the Al alloy of the FRM matrix and the Ti alloy was sufficient.

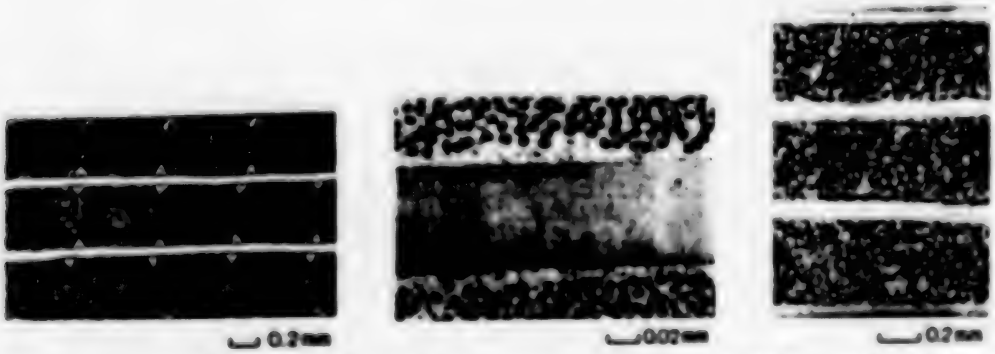

(a) M30/5056, Ti-3Al-2.5V (b) SiC(pcs)/1050, Ti-3Al-2.5V

Figure 7. Cross-Sectional Microstructure of Ti Alloy Hybrid Material

Table 2. Forming Conditions of Hybrid Material and Tensile Test Results

Preform	Forming conditions: Method	T_1 / T_2 (K)	t_1/t_2 (min)	P (MPa)	V_f / V_{f_1} (%)	Density (g/cm³)	Tensile strength 0° Aver.	Tensile strength 0° Min.	Modulus of elasticity 0° Aver.	Strain 0° Min.
M30/5056 + Ti-3Al-2.5V	Hot piston	843	5	39.2	40 17	2.6	696 656 723 (4)	151 142 161 (3)	142 140 143 (5)	0.61 0.55 0.66 (5)
SiC (pcs)/1050 + Ti-3Al-2.5V	Hot piston	813	30	39.2	31 17	2.9	795 783 811 (5)	186 165 206 (2)	112 112 113 (5)	>1.00 0.80 >1.07 (5)

( ) Figures in parentheses indicate number of samples.

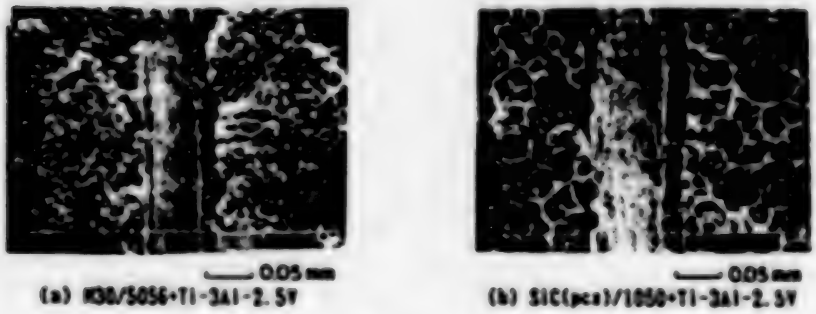

(a) M30/5056+Ti-3Al-2.5V (b) SiC(pcs)/1050+Ti-3Al-2.5V

Figure 8. Fracture Shape of Hybrid Material (After 0° direction tensile test)

5. Conclusion

This research has been conducted as part of the "Research and Development of Composite Materials" entrusted to the (Foundation) Association of Basic Technology for Future Metals and Composite Materials based on the Project of Basic Technology for Future Industries by the Agency of Industrial Science and Technology, MITI.

20158/9365

Tensile Properties of Matrix Composites by HIP Process

43063807J Tokyo DAIJUNIKAI FUKUGO ZAIRYO SYMPOSIUM (KOEN YOSHISHU) in Japanese 22-23 Oct 87 pp 165-168

[Article from day 2, session 18, by Kenichi Aota and Takashi Motoda, Kobe Steel, Ltd., Material Research Laboratory]

[Text] **1. Objective of Research**

Various composite materials have attracted attention as lightweight and high-strength new materials, and research and development on FRM (fiber reinforced metal) excelling in thermal resistance is being actively promoted as a sequel to the resin system. Since titanium is lightweight and excels in thermal resistance in comparison with aluminum, it is promising as a matrix for FRM. The HIP device, which is used in the solidification forming of metal powders and ceramics, is also effective as a means of diffused junction forming of FRM. Pressure forming by hydrostatic pressure is especially advantageous in the near-net forming and the forming of curved surface structure, and it is considered as a means of exhibiting its characteristics as a forming method of FRM in which secondary formability is difficult.

The combination of fiber and matrix is important in the forming of FRM. In this research, HIP forming was conducted wherein a thick-diameter CVD fiber which was advantageous to an active metallic titanium was combined with a representative Ti alloy matrix based on the results obtained in an interfacial reactivity test of the titanium alloy and various fibers.[1] Together with checking the strength characteristics and studying the effects exerted by the fiber and matrix, making the effectiveness of this forming method clear was the objective of this research.

2. Experiment Method

The chemical compositions of the reinforcing fibers and matrix alloys used in the experiment are shown in Tables 1 and 2. All matrixes used were representative Ti alloys; however, powder was used as the raw material as there were some cases in which the foil that is ordinarily used in FRM forming was not available. Powder less than 177 μ obtained by the rotating electrode method was sieved and used. The method of preparing the plate compacts by the powder HIP process is shown in Figure 1. The plate

Table 1. Reinforcing Fibers

	Diameter (μ)	Characteristics Strength (GPa)	Modulus of elasticity (GPa)
SiC(CVD)	140	3.5	400
B/B_4C(CVD)	140	4.0	370
B(CVD)	140	3.5	400

Table 2. Chemical Components (W/O) of Ti Alloy Powder

	Al	V	Sn	Zr	Mo	Fe	C	N	H	O	B	W.A
Ti-6Al-4V	6.00	4.12	—	—	—	0.10	0.017	0.011	0.0034	0.175	V 4.00	PREP
Ti-6Al-2Sn-4Zr-2Mo	6.10	—	2.00	4.12	2.00	0.10	0.008	0.013	0.0029	0.091	—	PREP
Ti-6Al-2Sn-4Zr-6Mo	6.07	—	2.05	4.10	6.01	0.10	0.007	0.012	0.0021	0.102	V 4.00	PREP

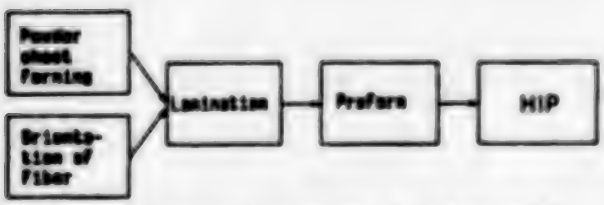

Figure 1. Preparation Method of Ti Substrate-Shaped Composite

laminates were prepared by alternately laminating five layers each of the powder plate that was formed to the prescribed thickness by using a binder and the orientation fiber mat that was wound by a winder at a fixed spacing and fixed by resin. After removing the binder, preforming was conducted at 900°C (15 minutes) 49 MPa using forming conditions studied in advance, the HIP processing was conducted at 950°C (1 hour) 98 MPa, and together with obtaining a unidirectional reinforced plate solidification compact and evaluating the tensile properties, microfiber observation and fracture observation were conducted and studies were made on these observations.

3. Experiment Results and Considerations

1) Effect of reinforced fibers on strength

The tensile strength of HIP compacts when using Ti-6Al-4V as the base and, respectively, the fibers SiC(CVD), B/B_4C(CVD), and B(CVD) is shown in Figure 2. The tensile strength at ordinary temperature is highest when it has been reinforced with SiC(CVD), whereas the tensile strength at ordinary temperature is low in the case of B/B_4C(CVD) and B(CVD). And the trend is

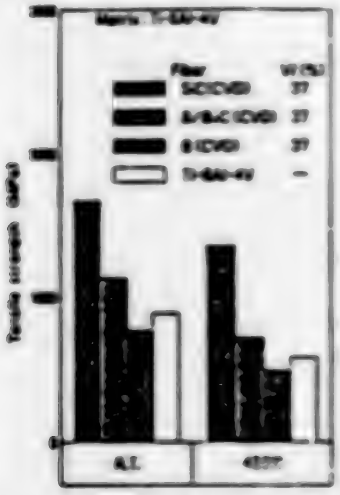

Figure 2. Effect of Fiber on Strength

the same at a temperature of 450°C. The tensile strength of B(CVD) is also lower than a fiber that has been HIP formed with the simple substance Ti-6Al-4V, so strength improvement cannot be expected from the B(CVD) fiber.

Fibers observed by SEM (scanning electron microscope) on the interfacial part of various fibers after forming are shown in Figure 3. The reaction layer of SiC(CVD) is thin, about 0.8 μ, and the surface of the interfacial reaction layer is smooth. The reaction layer of B/B_4C(CVD) is thick, about 2 μ, and the surface is in a needle-shaped condition. The reaction layer of B(CVD) is thicker, about 3.5 μ, and the surface is in a needle-shaped condition.

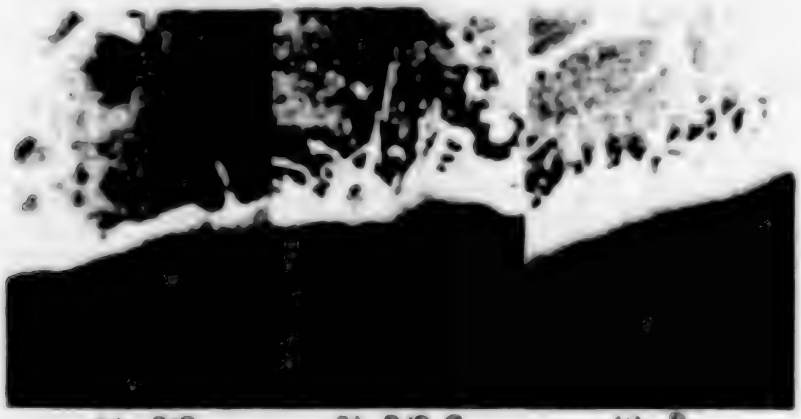

(a) SiC (b) B/B_4C (c) B

Figure 3. Interfacial Reaction Layer of Various Fibers of Compacts (Matrix: Ti-6Al-4V)

The SEM observed structure after the tensile test is shown in the upper row of Figure 4. In the SiC(CVD) fiber, a separation has been generated between the main fiber body and the generated interfacial reaction layer or the carbon rich layer of the fiber. In the B/B_4C(CVD) fiber, a separation has also been generated between the interfacial reaction layer and the

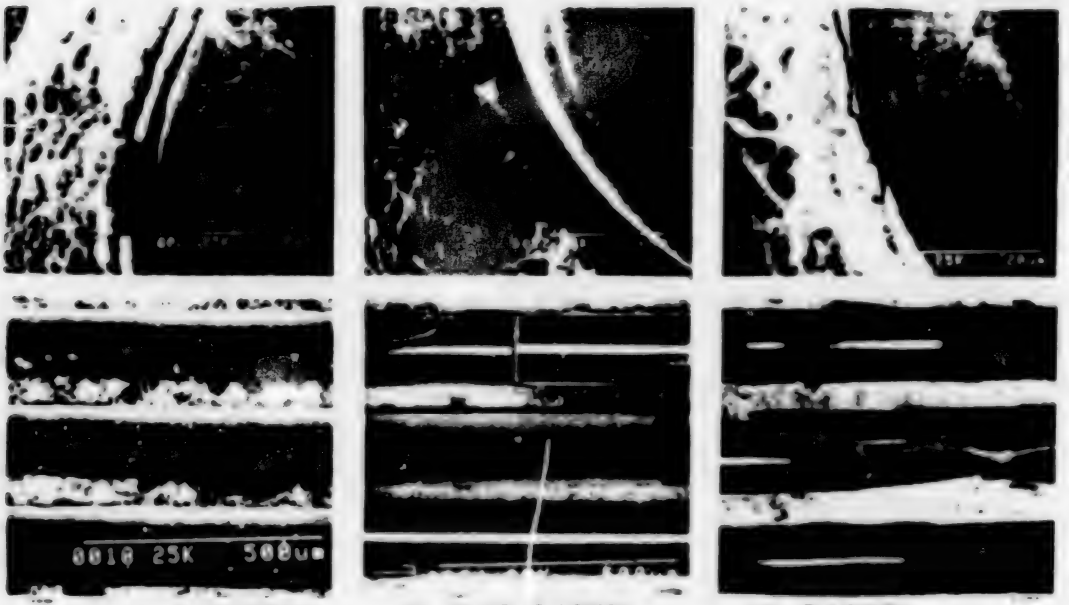

(a) SiC (CVD) (b) B/B_4C (CVD) (c) B (CVD)

Figure 4. Structure After Tensile Fracture (Upper row 0°, lower row 90° direction, matrix: Ti-6Al-4V)

fiber. In the B(CVD) fiber, a severe crack has been generated in the interfacial reaction layer, and an aspect has been assumed in which the crack has developed and passed through the fiber and reached fracture.

Ochiai, et al.,[2] studied the relationship between the interfacial reaction layer and strength using a single fiber model. They found that a crack generated in the reaction layer easily advanced to the main fiber body and the strength deteriorated when the adhesive strength of the reaction layer and fiber was great, whereas the development of fracture was prevented by the separation of the interface and a deterioration was not generated when the adhesive strength of the reaction layer and fiber was small. They reported that the development of a crack occurred under conditions of lower stress as the thickness of the interfacial reaction layer was increased. Tensile fracture in a perpendicular direction to the compact fiber of various fibers is shown in the lower row of Figure 4. All SiC(CVD)/ fibers were fractured at the interface with the fiber. In the case of the B/B_4C(CVD) fibers, some were found to be the same as the SiC(CVD)/ fibers and some were found to be divided in two at the central part of the main fiber body. In the case of B/(CVD) fibers, all were fractured at the main fiber body and not at the interface. Thus, it is considered that the degree of adhesion between the fiber and the reaction layer is greatest in the B/(CVD) fibers, followed in order by the B/B_4C(CVD) fibers and then the SiC(CVD) fibers. It is judged that a crack develops most easily in the SiC(CVD) fibers, if we consider that the ease of development of a crack from the interfacial reaction layer also follows the same order as the degree of adhesion [sic]. Since the interfacial reaction layer is least thick in the SiC(CVD) fibers and becomes thicker in order in the B/B_4C(CVD) and B/(CVD) fibers, it is considered that the SiC(CVD) fiber necessitates

the highest stress value for the generated crack to develop. Furthermore, since the shape of the interfacial reaction layer is comparatively smooth in the SiC(CVD) fibers and in a needle-shaped condition in the B/B_4C(CVD) and B/(CVD) fibers, it is assumed that it is difficult to generate a crack in the reaction layer in the SiC(CVD) fibers. Therefore, it is considered that the strength of the reinforced compact is highest in SiC(CVD) fibers, followed in order by B/B_4C(CVD) and B/(CVD) fibers.

2) Effect of matrix alloy on strength

The tensile strength of HIP compacts using SiC(CVD) fiber and, respectively, the bases Ti-6Al-4V, Ti-6Al-2Sn-4Zr-2Mo, and Ti-6Al-2Sn-4Zr-6Mo alloys is shown in Figure 5. The tensile strength at ordinary temperature was the highest in Ti-6Al-2Sn-6Mo and it coincided with the matrix strength in order of Ti-6Al-4V and Ti-6Al-2Sn-4Zr-2Mo; the compacts of all the alloys showed strength of more than 1,470 MPa (150 kg/mm^2). The tensile strength at 300°C and 450°C also exhibited the same trend; the Ti-6Al-2Sn-4Zr-6Mo, especially, had a strength of more than 1,470 MPa (150 kg/mm^2) at 450°C, and expectations could be harbored as to its strength particularly on the high-temperature side. A comparison between the elastic modulus of a compact using various matrixes and the compounding rule (ROM) is provided in Table 3. It is more than 200 GPa, about twice that of the Ti alloy in all cases. The forming efficiency against the compounding rule is about 90 percent, showing no great difference among the matrixes, and the forming efficiency against strength was also the same. Since there is no great difference in forming efficiency in the range of this alloy, it is considered on the basis of the points mentioned above that it follows the order of strength of the matrix alloys. The adaptability of the alloy system containing Zr and Mo was high in regard to the interfacial reaction layer[1]; since no great difference in strength is generated among the matrixes in regard to forming efficiency, as seen in this result, it is considered that using a high-strength matrix is effective for high strengthening of compacts and that a direction has been provided for the improvement of thermal resistance which is the forte of FRM.

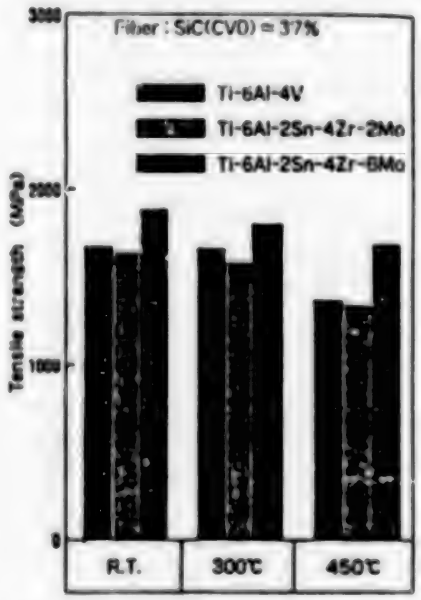

Figure 5. Effect of Base Alloy on Strength

Table 4 shows the various tensile properties of plate compacts. The tensile property values in the 90° direction are high for Ti-6Al-2Sn-4Zr-6Mo, which is a high-strength matrix. It can also be seen from this table that tensile strength in the 90° direction is about 400 MPa for the Ti base compacts--far higher than the ordinary values of Al base compacts of the same type, which is about 100 MPa. Figure 6 shows a tube that has been

Table 3. Modulus of Elasticity and Forming Efficiency of Ti Base FRM

	Ti-6Al-4V	SiC(CVD) Ti-6Al-2Sn-4Zr-2Mo	Ti-6Al-2Sn-4Zr-6Mo
Volume fraction (percent)	37	37	37
Modulus of elasticity (GPa)	205	203	218
Compounding (ROM) rule (GPa)	225	228	231
Forming efficiency (percent)	91	89	94

Table 4. Mechanical Properties of SiC(CVD)/Ti FRM Unidirectional Plate-Shaped Compacts

Direction	Measured items \ Alloy	Ti-6Al-4V	Ti-6Al-2Sn-4Zr-6Mo
0°	Tensile strength (MPa)	1,752	1,840
	Modulus of elasticity (GPa)	208	223
	Poisson's ratio	0.24	0.26
90°	Tensile strength (MPa)	371	416
	Modulus of elasticity (GPa)	147	156
	Poisson's ratio	0.17	0.18

Figure 6. Appearance of Tube-Shaped Body of Ti Base FRM Formed by HIP (SiC(CVD)/Ti-15Mo-5Zr-3Al, TS: 1,774 MPa)

formed in a shape making the most of the HIP forming method forte by using a high-strength Ti-15Mo-5Zr-3Al of the β alloy system among the Ti alloys; it is comparatively easy to process into a foil that is easy to use in the

forming of FRM. The axial direction tensile strength of a specimen cut out from the tube was 1,774 MPa (180 kg/mm^2) at room temperature, superior characteristics were available, and it was demonstrated that the HIP forming method was effective in the forming of Ti base FRM.

4. Conclusion

The effects of fiber matrix alloys on the strength of FRM compacts formed by the HIP forming method by combining various CVD fibers and Ti alloys were studied. It was ascertained that a higher strength was available in the SiC(CVD) fiber than in the B/(CVD) and B/B_4C(CVD) fibers, and that it was advantageous to use a high-strength matrix as there was no great difference in the forming efficiency among the matrix alloys. At the same time, it was demonstrated that the HIP forming method, which is known to necessitate a comparatively high temperature and long time in forming, was useful in the forming of FRM. This research has been conducted as part of the "Research and Development of Composite Materials" entrusted to the (Foundation) Association of Basic Technology for Future Metals and Composite Materials based on the Project of Basic Technology for Future Industries by the Agency of Industrial Science and Technology, MITI.

References

1. Aota, et al., IRON AND STEEL, Vol 71, 1985, p S1615.

2. S. Ochiai, et al., MET. TRANS., Vol 12A, 1981, p 1155.

20158/9365

Fabrication Method of SiC Whisker Reinforced Al Composites

43063807k Tokyo DAIJUNIKAI FUKUGO ZAIRYO SYMPOSIUM (KOEN YOSHISHU) in Japanese 22-23 Oct 87 pp 169-172

[Article from day 2, session 19, by Akira Sakamoto, Hideto Hasegawa, and Makoto Senda, Mitsubishi Heavy Industries, Ltd., Nagoya Aircraft Works]

[Text] 1. Outline

Development of liquid infiltration and extrusion processes has been promoted on SiC whisker/Al system FRM. Defects caused by cluster-shaped whiskers, lump-shaped special objects, etc., occurring in the production of whiskers or defects such as shrinkage porosity generated during liquid infiltration molding remain after extrusion molding in FRM of this system, and they are the main causes of lowering the strength characteristic of FRM. Measures such as the refining of whiskers and liquid phase HIP treatment of the liquid infiltration compacts were studied as means for solving these defects, and the basis of a liquid infiltration and extrusion forming technology was established for FRM of this system.

2. Molding Process

Since cluster-shaped whiskers, lump-shaped special objects, etc., were intermingled among the whiskers (Figures 1 and 2) and remained as defects in the compact even after the liquid infiltration and extrusion molding processes, a "hydrofluoric acid treatment" and "underwater sedimentation treatment" were performed as whisker refining treatment prior to preform molding. The majority of foreign matter was removed, but a portion still remained (Figure 3). Together with the presence in the compact of scattered foreign matter that could not be completely removed by such refining of whiskers, there were defects such as shrinkage porosity, generated concentratedly in the bottom part of a compact which becomes the final solidifying domain of the liquid infiltration in liquid infiltration molding. These defects could not be made to disappear even by extrusion molding (Figure 10). However, such defects as shrinkage porosity remaining in the compact were made to practically disappear by providing a liquid phase HIP treatment under the conditions of matrix solidus line + 70 K, 147 MPa for 30 minutes for the liquid infiltration compact (Figure 4). As a result of performing hot isothermal extraction by using the liquid infiltration formed billets to which the liquid phase HIP treatment had

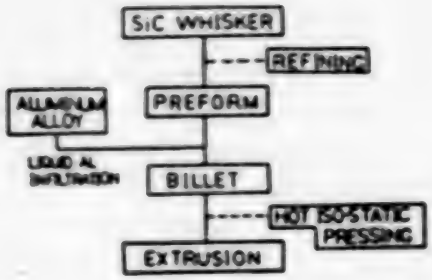

Figure 1. Liquid Infiltration and Extrusion Molding Process of SiC(W)/Al System

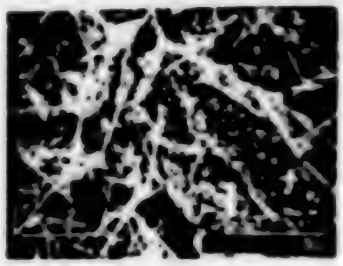

Figure 2. Acquisition Condition of Tested Whiskers

Figure 3. Refining Treatment Condition of SiC Whiskers

Table 1. Characteristics of Tested Whiskers

	Characteristic values
Diameter (μm)	0.05 - 1.5
Length (μm)	20 - 200
Aspect ratio	20 - 200
Density (Mg/m³)	3.18
Grade	#1-S-SF-SU

In accordance with catalog values of manufacturer

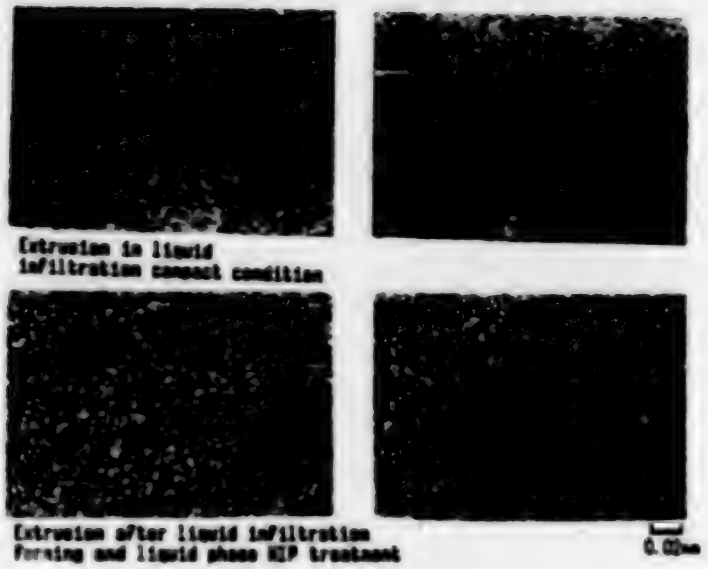

Figure 4. Sectional Microstructure of Liquid Infiltration Compacts (SiC(W)/Al7075, V_f = 0.25)

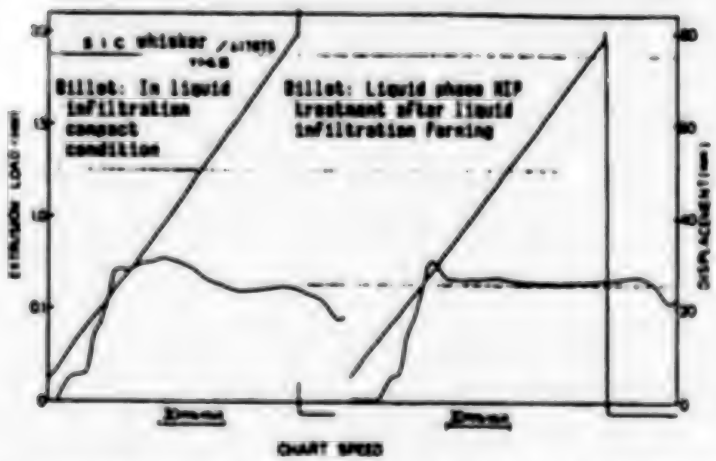

Figure 5. Relationship of Extrusion Speed and Displacement Vs. Chart Speed of SiC(W)/Al7075

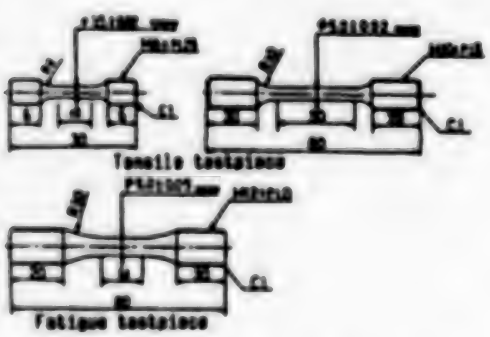

Figure 6. Shape of Testpiece

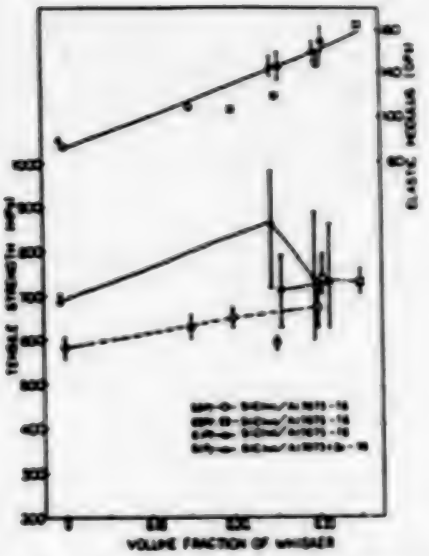

Figure 7. Relationship of Tensile Strength, Elastic Modulus and Volume Fraction (V_f) of Whisker of Extrusion Compact

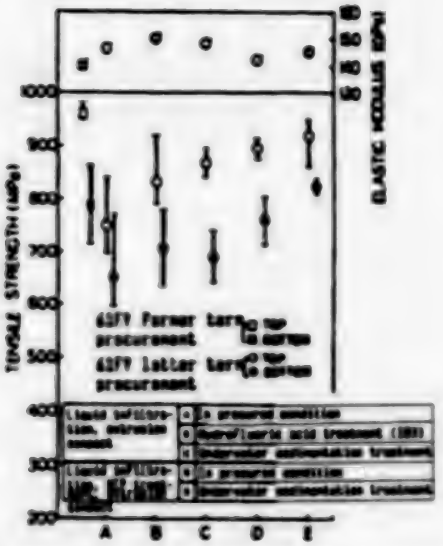

Figure 8. Relationship Between Tensile Strength and Whisker Refining Treatment of SiC(W)/7075 + Zn Extrusion Compact

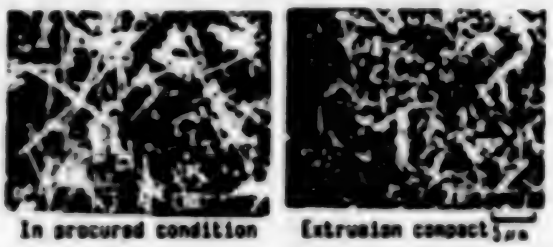

Figure 9. Forms of Extrusion Whiskers

Figure 10. Tensile Fracture and Sectional Microstructure of Extrusion Compacts

been applied, there was no generation of defects such as tearing on the surface of the extruded materials, and it was demonstrated that this HIP treatment also had an effect in improving the extruding property.

3. Mechanical Characteristics of SiC Whisker/Al 7075 System FRM

The various characteristics such as tensile strength and fracture toughness (grouped together by the Mechanical Technology Research Laboratory) and fatigue were evaluated on extruded materials that used the 7000 system Al alloy for the matrix material and to which the molding process mentioned in section 2 above had been applied (Figures 6 to 13). The tensile strength at room temperature showed a saturation tendency at a fiber volume fraction (V_f) of 25 to 30 percent, and the maximum of 1,078 MPa was indicated. As to the tensile strength at high temperature, the 473 K strength of FRM was almost equivalent to the room temperature strength of the matrix material; the strength of the materials that underwent HIP treatment was about 500 K higher than those without such treatment; and the room temperature strength had effectively been improved. The fatigue strength was greatly affected by defects in the compact; such liquid phase HIP treatment may also be effective for improving the fatigue strength together with refining the whiskers. A specific strength and specific elasticity equivalent to that of the continuous fiber SiC(pcs)/Al are available in FRM extruded materials by this process (Figure 14).

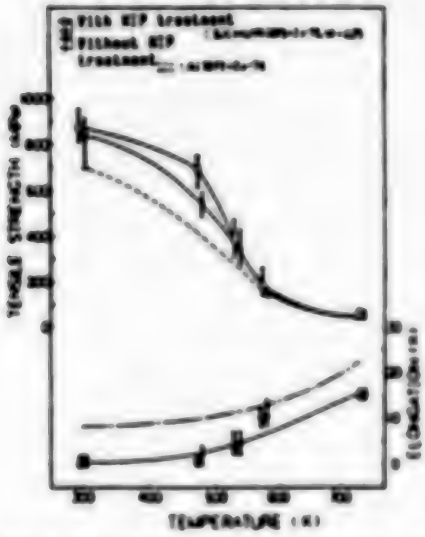

Figure 11. High-Temperature Strength Characteristics of SiC(W)/Al7075 + Zn Extrusion Compact

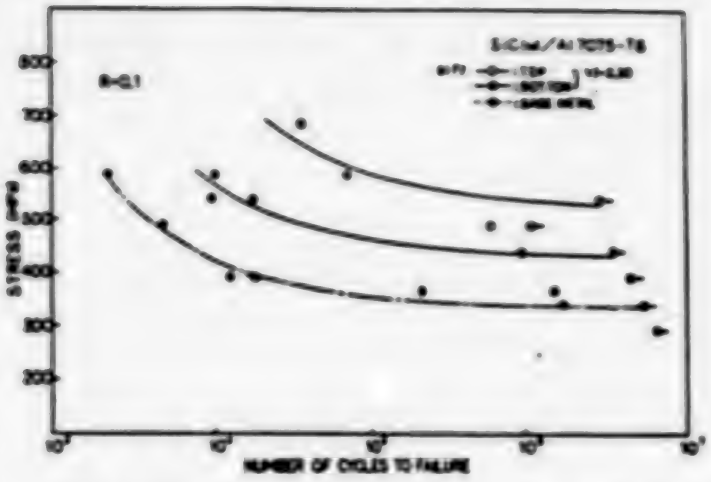

Figure 12. Fatigue Characteristics of SiC(W)/Al7075 Extrusion Compact

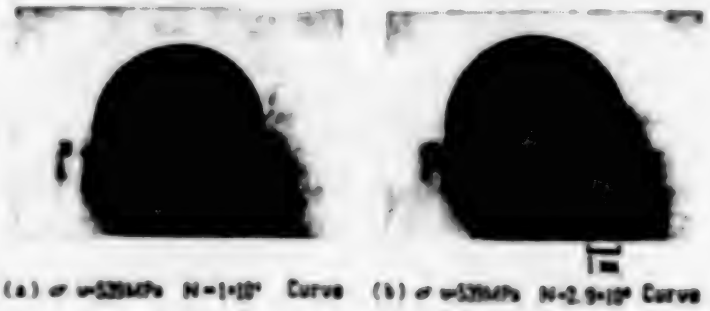

Figure 13. Fatigue Fracture of Extrusion Compact (SiC(W)/Al7075-T6, V_f = 0.30)

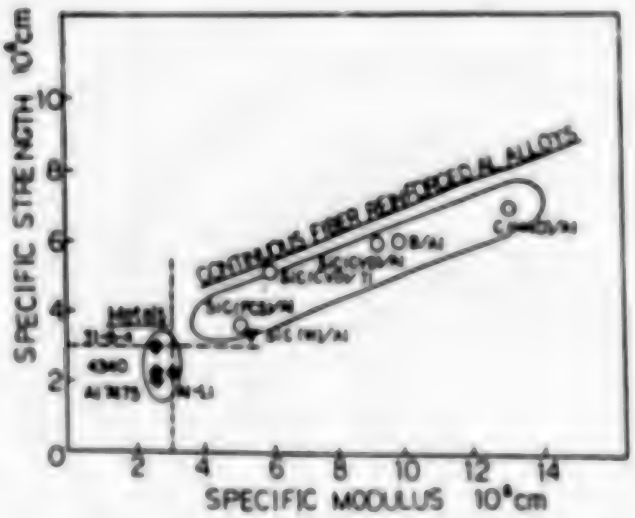

Figure 14. Positioning of SiC(W)/Al System FRM

This research has been conducted as part of the "Research and Development of Composite Materials" entrusted to the (Foundation) Association of Basic Technology for Future Metals and Composite Materials based on the Project of Basic Technology for Future Industries by the Agency of Industrial Science and Technology, MITI.

20158/9365

Strength Properties of SiC-Al Composites Fabricated by HP

430638071 Tokyo DAIJUNIKAI FUKUGO ZAIRYO SYMPOSIUM (KOEN YOSHISHU) in Japanese 22-23 Oct 87 pp 173-176

[Article from day 2, session 20, by Sotohiro Takabayashi, Central Research Institute, Toyama Industrial Technology Center]

[Text] 1. Introduction

Since aluminum that has compounded whiskers has a high specific strength and excels in impact resistance characteristics in comparison with FRP, expectations are harbored for it as a future structural material. In this research, the compounding of the SiC whiskers and 2014 aluminum alloy was accomplished by hot pressing (HP), and the high-temperature flexural strength characteristics were studied. Whiskers were unidirectionally oriented by extrusion molding, and the tensile strength and thermal expansion characteristics were investigated.

2. Experiment Method

The whiskers were first ultrasonically agitated in organic solvent, and the 2014 aluminum alloy was mixed in. The fiber volume fraction (V_f) of whiskers was weighed then, and it was 0, 0.15, and 0.25. β-SiC_w made by the Tateho Chemical Co., Ltd., was used for the whiskers, and the 2014 aluminum alloy was made by the Nippon Light Metal Co., Ltd. The whisker and aluminum alloy mixture was dried at 432 K (in air), inserted into a 50 mmϕ carbon mold, and hot pressing was performed in argon atmosphere. After being maintained at a temperature of 963 K and pressure of 20 MPa for 1,200 seconds under hot pressing, it was cooled. Billets were processed to 30 mmϕ and 50 mm thickness by a lathe (carbide tool) and further processed to 7 mmϕ by hot extrusion. The extrusion conditions in this case were a temperature of 753 K and extrusion rate of 6.7 mm/sec. Since the 2014 alloy is a material that is subject to age hardening, in this experiment the composite material was subjected to a T6 treatment (773 K-7 K sec, water quenching, 443 K-36 K sec), and the effect was examined.

A 3 x 4 x 40 mm sample was cut by a CC grindstone, and a three-point flexural test (room temperature to 673 K) was conducted. The testing speed was 8.3 μm/sec, and a high-temperature test was conducted 600 seconds later after reaching the prescribed temperature. The tensile test was conducted

by processing the sample to 3 mmφ with a lathe at a technology rate of 16.7 μm/sec. The thermal expansion measurement was conducted at the temperature increase rate of 0.18 K/sec.

3. Experiment Results and Considerations

1) Three-point flexural strength

The relationship between the temperature and three-point bending stress for each V_f is shown in Figure 1. The sample was treated with a T6 treatment. A strength of 1,000 MPa was recorded at approximately room temperature at a V_f of 0.15. Compared with the 2014 alloy, this demonstrates an improvement in strength of about 20 percent. The effect of whisker compounding becomes evident as the temperature becomes higher. For example, compared with the 2014 alloy, the flexural strength was more than double at V_f 0.25 and it was more than 1.5 times at V_f 0.15 at a temperature of 673 K (400°C). Furthermore, it is known that the greater the V_f, the higher the temperature required to cause a drop in strength. This is because the reinforcement effect is increased when there are many whiskers, as whiskers that are strong against heat are reinforcing the softened aluminum. The strength of a sample with a fiber V_f of 0.15 is higher than a sample with a fiber of 0.25 at room temperature, and this because the cohesive factor--i.e., the probability of defects entering--rises when the fiber V_f rises, as whiskers are susceptible to cohesion. Since the fracture form at approximately room temperature is controlled by the brittle fracture of the matrix, a sample with a fiber volume fraction of 0.25 with many defects is more brittle at room temperature. However, it can be considered that the strength of a sample with many whiskers becomes higher as ductile fracture is generated when the temperature becomes high [sic].

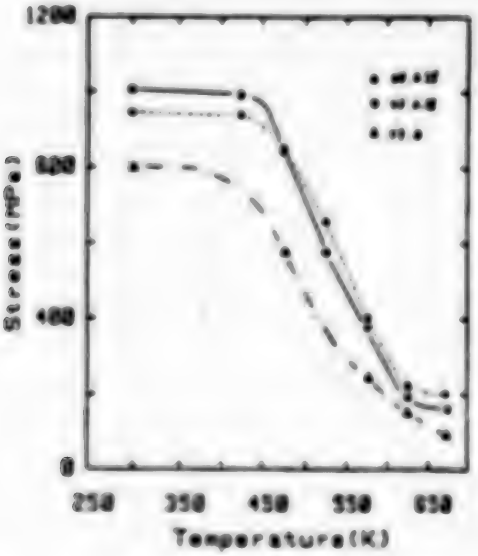

Figure 1. Bending Stress of Composites

2) Tensile strength

It is known that the whiskers in an extruded sample are gradually oriented in the extruded direction, as shown in Figure 2. The aspect ratio of the finally extruded part was 6 to 10 for the sample with a fiber V_f of 0.15, and it was 3 to 8 for the sample with a fiber V_f of 0.25. Since the aspect ratio before extrusion was 15 to 20 whereas that before mixing was 20 to 200, it was demonstrated that the whiskers were broken to pieces at mixing and hot pressing, and they were further broken in two by extrusion. Moreover, the higher the V_f, the easier the fracture of whiskers and the lower the aspect ratio becomes.

Figure 2. SEM Photographs of Extruded Composites

The tensile strength is shown in Table 1. The condition of fracture after the tensile test is shown in Figure 3. Compared with aluminum alloy, in a sample with the whiskers unidirectionally oriented a little more than double the strength was shown at V_f 0.15, and a little more than triple the strength was shown at V_f 0.25. The phenomenon of the strength dropping in a sample with a larger V_f--such as occurred in the three-point flexural test--was not observed, and the compounding effect of the whiskers appeared intact. Thus, it is considered that the sample with a higher V_f demonstrated a higher compounding effect, as the defects existing in the sample interior had been removed by the extrusion process.

Figure 3. SEM Photograph of Extruded Composite After Tensile Test

Table 1. Tensile Stress of Composites

Volume fraction of fiber	Hot extrusion	Heat treatment T6	Tensile stress σ (MPa)
0			160
0.15	o		370
0.15	o	o	590
0.25	o		500
0.25	o	o	640

3) Thermal expansion coefficient

The thermal expansion coefficient of various samples is shown in Figure 4. The thermal expansion coefficient of a sample that has undergone extrusion becomes small in the neighborhood of 600 K, and it becomes large again in the neighborhood of 640 K. This is considered to be due to the residual stress generated by the extrusion process becoming released by the softening of the aluminum at a high temperature. The coefficient of linear expansion of the various samples is shown in Table 2.

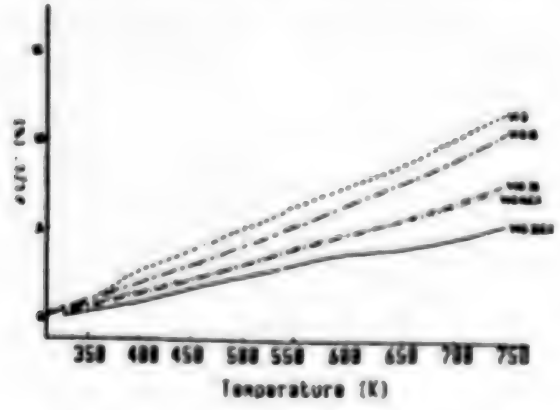

Figure 4. Thermal Expansion Coefficient of Samples

Table 2. Linear Thermal Expansion Coefficient of Composites

Specimen	Linear thermal expansion coefficient $\alpha(\times 10^{-6}/K)$	Temperature (K)
V_f 0	25.9	323-723
V_f 0.15	23.3	"
V_f 0.15 extruded	16.0	"
V_f 0.25	17.3	"
V_f 0.25 extruded	12.3	"

thermal expansion, as seen here, can be fairly well held down by the compounding effect of the whiskers. Thermal expansion in the extruded direction can be further held down by performing the extrusion process; a value of $1 - 12.3 \times 10^{6}/K$--that is, less than half of the matrix aluminum--was obtained in a sample of V_f 0.25.

4. Conclusion

The following was demonstrated in this experiment.

1. Whiskers could be homogeneously dispersed in SiC_w-Al composite materials prepared by hot pressing.

2. The compounding effect of the whiskers was evident at high temperature.

3. In the extrusion process, the whiskers can be unidirectionally oriented, and it is considered that the internal defects generated during hot pressing are removed.

4. The thermal expansion coefficient can be held down by compounding the whiskers.

References

1. Manuscripts of Third Basic Technology for Future Industries Symposium, 1985.

20158/9365

Evaluation of FRM High-Temperature Tensile Strength

43063807m Tokyo DAIJUNIKAI FUKUGO ZAIRYO SYMPOSIUM (KOEN YOSHISHU) in Japanese 22-23 Oct 87 pp 177-180

[Article from day 2, session 21, by Kazumi Hirano and Tsutomu Sasaki, Mechanical Engineering Laboratory, Agency of Industrial Science and Technology]

[Text] **1. Introduction**

Research and development has been actively promoted recently on fiber reinforced metals (FRM) that aim at high strength, high toughness, and superior thermal resistance properties. Besides the specific strength and specific modulus of elasticity that are peculiar to composite materials, special expectations are harbored for the thermal resistance of FRM, as compared with FRP (fiber reinforced plastics), as the matrix of FRM is metal. Of course, FRM has many defects as well as advantages; there is a drop in strength resulting from the formation of a reaction embrittlement layer, which is mainly caused by an interfacial control problem between the reinforced fiber and the matrix at manufacture. Therefore, the point of how to achieve a high specific strength and high modulus of elasticity by solving this problem becomes one of the points in evaluating mechanical characteristics of FRM. In this research, studies were conducted on matters related to the fracture mechanism in the mechanical properties of unidirectional continuous fiber reinforced metals aimed at the development and standardization of performance evaluation technologies such as the evaluation standard and characteristic testing method of FRM.

2. Materials and Experiment Method

2.1. Shape and size of specimen and testpiece

The materials used in this experiment were unidirectional continuous fiber reinforced metals. The reinforced fibers were carbon fiber (CF), carbon silicide fiber (SiC(CVD)) prepared by the chemical vapor deposition method, and Nicalon fiber (SiC(pcs)) and the matrix metals can be largely classified as aluminum alloy and titanium alloy.

The testpiece used was a plate-shaped testpiece having a parallel part; a tab was attached to the chuck part in the room-temperature test, and a

stainless mesh was spot welded in the high-temperature test. The shape and dimensions of these testpieces are shown in Figure 1. As a rule, the thickness was made the original thickness of the compact, and the surface of the testpiece was finished with #1000 emery paper.

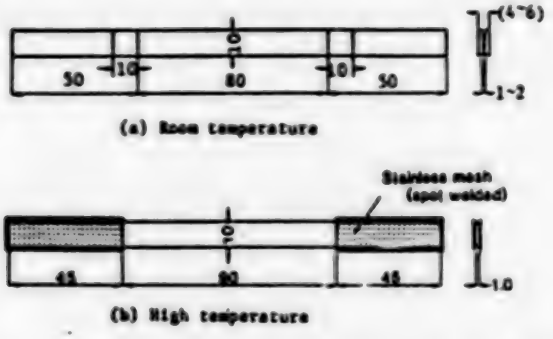

Figure 1. Shape and Dimensions of Testpiece

2.2. Test method

(1) Room temperature test

An autograph (capacity 49 KN) prepared by the Shimadzu Corp. was used for the room temperature tensile test, which was conducted in room temperature atmosphere with the crosshead speed fixed (0.1 to 1 mm/min). Strain measurement was made by two methods--one method using an extensometer with a gauge length of 50 mm, and the other using a strain gauge with a base dimension of 5 x 3 mm. The modulus of direct elasticity E was made the tangent modulus which was defined by the inclination $\Delta\sigma/\Delta\epsilon$ of the stress σ-strain ϵ curve in a certain optional stress level. The tensile strength 6_{UTS} was obtained by dividing the maximum tensile load by the sectional area, and the fracture strain ϵ_f was defined as the strain against the tensile strength 6_{UTS}.

(2) High-temperature test

An infrared furnace was used for the high-temperature tensile test, and the test was conducted after heating the furnace to the prescribed temperature and maintaining it in this condition for 5 to 10 minutes. As in the room temperature test, it was conducted at a fixed crosshead speed in a temperature range up to 600°C. The temperature distribution of the testpiece parallel part in this case was in the range of ±5°C. The strain measurement was made by using the trial-manufactured high-temperature extensometer with a gauge length of 30 mm, as shown in Figure 2.

3. Results and Considerations

(1) Strain dependency on the modulus of direct elasticity

The strain dependency on the modulus of direct elasticity is shown in Figure 3. Since it was confirmed experimentally that there was almost no

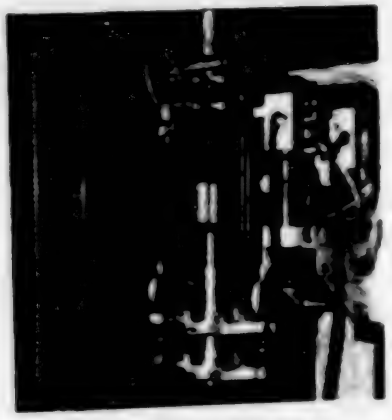

Figure 2. Trial-Manufactured High-Temperature Extensometer

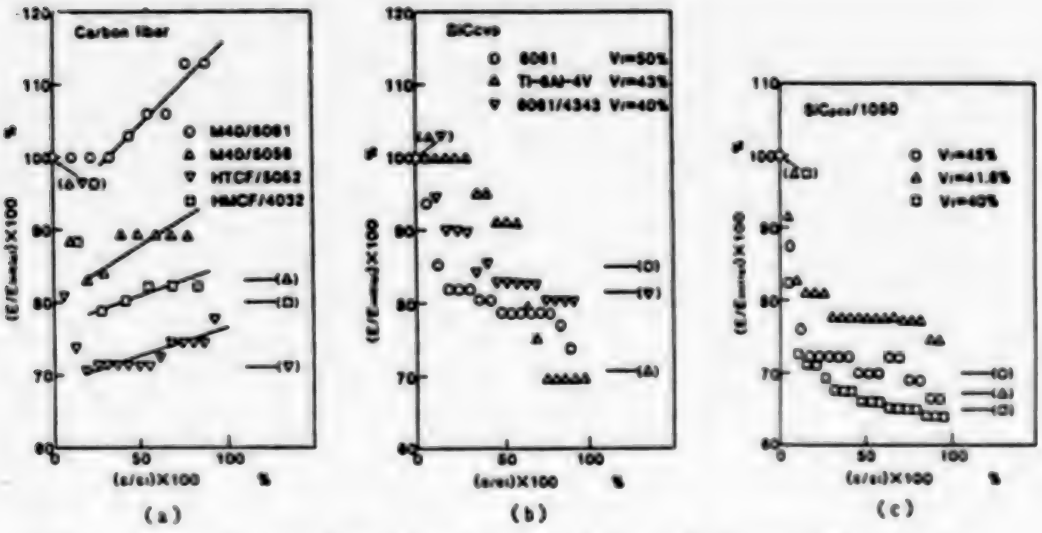

Figure 3. Strain Dependency on Modulus of Direct Elasticity

difference in the σ-ϵ curve measured by the extensometer method and the strain gauge method, the nondimensionalized elastic modulus (E/Ea) divided by the initial modulus of direct electricity (Ea) in 6-0 was obtained based on the σ-ϵ curve by the strain gauge method, and it was plotted against ϵ/ϵ_f. The strain dependency of the modulus of direct elasticity differs according to the type of reinforced fiber, the fiber volume fraction V_f, the type of matrix metal, and the production method. Moreover, the microscopic fracture mechanism in the neighborhood of fracture also plays a part. In the case of the CF fiber reinforced metal shown in (a), ϵ/ϵ_f rises inversely from the range of 20 to 30 percent after the sudden decrease of E/Ea with the increase of strain. The initial increase of E/Ea is understood as the decrease in the matrix contribution part exerted on the modulus of direct elasticity of the composite material, which is expressed by the compounding rule of the following formula as a result of the plastic deformation of the matrix metal.

$$E_c = E_f + (1 - V_f) E_a \qquad (1)$$

Here, E_f: modulus of direct electricity of reinforced fiber; V_f: volume fraction of reinforced fiber; E: modulus of direct elasticity of matrix metal. By the way, the value of E_c when $(1-V_f)Ea$ in formula (1) above is made zero coincides well with the minimum value of E/Ea as shown in parentheses in the figures. Moreover, the E/Ea rise after the disappearance of the matrix metal contribution is the appearance of the strain dependency of the CF fiber itself, and it is considered as resulting from the change in the microscopic system structure. Therefore, the rise rate differs according to the CF fiber type and according to V_f when of the same type. On the other hand, the E/Ea of the SiC/(CVD) fiber reinforced metal shown in (b) and of the SiC(pcs) fiber reinforced metal shown in (c) suddenly decreases with the strain increase, and after exhibiting an approximately fixed value in a certain strain range, it reaches fracture. The initial lowering of E/Ea, as in the CF fiber-reinforced metal, is understood as the disappearance of the matrix contribution part exerted on Ec with the plastic deformation of the matrix metal. This is also clear from the fact that the E/Ea of SiC/(CVD)/Ti-6Al-4V, which has titanium alloy as its matrix, exhibits an approximately fixed value in the $\epsilon/\epsilon_f < 30$ percent range. Moreover, E/Ea shows an approximately fixed value up to the neighborhood of fracture after the disappearance of the matrix metal contribution. This results from the fact that there is no strain dependency on the modulus of direct elasticity of the SiC(CVD) and SiC(pcs) fibers themselves. The lowering of E/Ea in the neighborhood of fracture by the increase of V_f is understood as the change in compliance caused by the generation of microcracks accompanied by fiber fracture.

(2) Strength achievement rate

The strength achievement rate against strength 6_B(ROM) computed from the compounding rule (ROM) is shown in Figure 4. The strength $6B_B$(ROM) is computed by the following formula:

$$6_B(\mathrm{ROM}) = 6_f \cdot V_f + (1-V_f)\, 6_m \qquad (2)$$

Here, 6_f and 6_m, respectively, show the tensile strength of the reinforced fiber and the tensile strength of the matrix metal. The value of Ea mentioned above coincides well with E, (E(ROM)), which has been computed from the compounding rule (ROM) of formula (1) (E/E(ROM) = 1.0), and an ideal compounding has almost been achieved in regard to the modulus of direct elasticity. In contrast, the $6_B/6_B$(ROM) is somewhat less than 1.0, and it is difficult to say that an ideal compounding has been achieved in regard to the tensile strength.

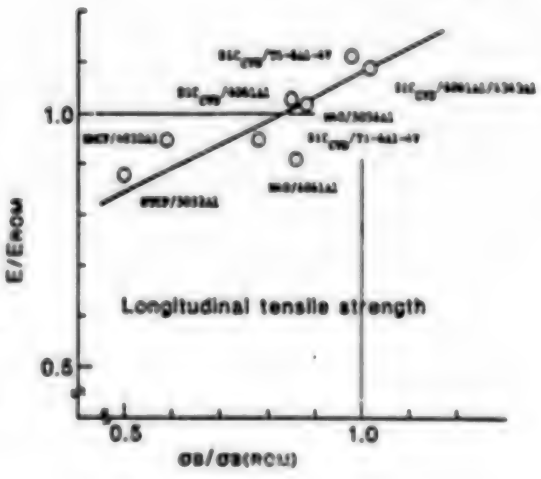

Figure 4. Strength Achievement Rate Against ROM Value

3.2. High-temperature tensile properties

(1) Stress-strain curve

A measured examine of the σ-ϵ curve at high temperature on SiC(CVD)/Ti-6Al-4V is shown in Figure 5. It closely resembles, for the most part, two straight lines also in all testing temperatures. The strain range of E_1 becomes small with the rise in the testing temperature, and the strain range of E_2 dependent only on the modulus of direct elasticity of the reinforced fiber becomes large. It corresponds with the mechanical characteristic change of the matrix metal at high temperature, and it is understood as the decrease of the matrix metal contribution part to E_1. It can be explained basically by the compounding rule, as in the room temperature tensile properties.

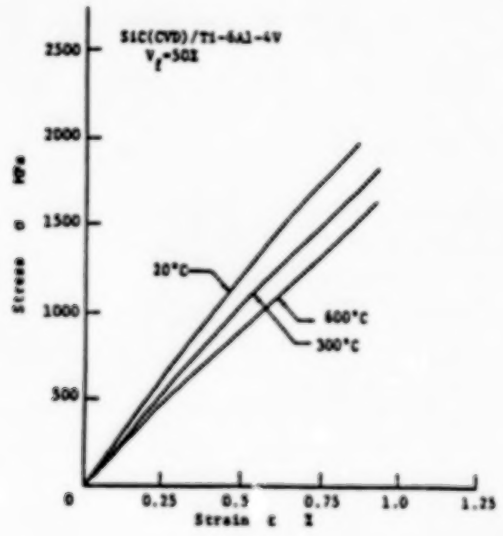

Figure 5. Comparison of Stress-Strain Curve at High Temperature

(2) Temperature dependency of mechanical characteristics

The temperature dependency of the modulus of direct elasticity, the tensile strength and the fracture strain on SiC(CVD)/Ti-6Al-4V is shown in Figure 6. The value of E_1 becomes small with a temperature rise and the decrease in the contribution part of the matrix metal. On the other hand, E_2 shows an almost fixed value in $T \lesssim 600°C$. It is a natural result when considering the temperature dependency of the modulus of direct elasticity of the SiC(CVD) fiber itself. Moreover, the tensile strength σ_{UTS} decreases with temperature rise. It coincides in trend with the temperature dependency of the matrix metal strength, and as in the change of E, it is understood as the decrease in the contribution part of the matrix metal. Furthermore, fracture strain ϵ_f exhibits an almost fixed value, and no temperature dependency is shown in practice.

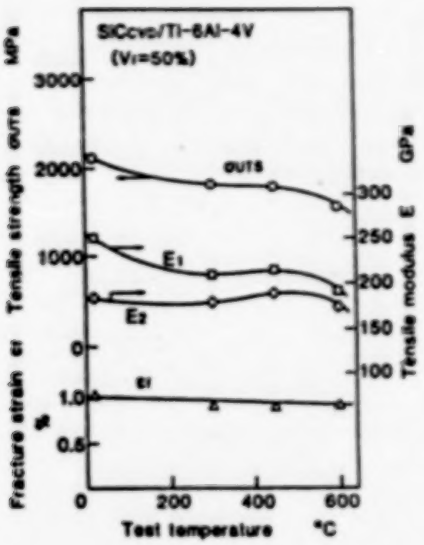

Figure 6. Temperature Dependency of Mechanical Characteristics

3.3. Fractographic observation

Based on fractographic observation of fractures, vertical tension type fractures were microscopically present in all materials; the drawing out of fibers was not obvious. Only the separation of the fiber and matrix was relatively conspicuous in the material system with a comparatively inferior strength achievement rate. A separation was generated conspicuously on the preform wire boundary surface in the case of SiC(pcs)/1050Al. Therefore, an apparent stress concentration phenomenon was generated during the tensile test due to the unbalancing of the load burden. It is considered that the strength achievement rate became inferior as a result of the wire preform defects and surface defects emphasized during wire preform production. In the case of the SiC(pcs) fiber reinforced composite materials, it is considered that prevention of separation of the wire preform boundary surface is the means of improving the strength. The fractographic observation of fractures in SiC(CVD)/Ti-6Al-4V at room temperature (20°C) and at 600°C is shown in Figure 7. Although slight differences are seen in the dimple-shaped fracture forms (size of dimple diameter, etc.) of the matrix metal, as can be conjectured from the temperature dependency of the mechanical characteristics of the matrix metal, the basic fracture mechanism is almost the same in $T \leq 600°C$. Also, almost no difference was discerned in the interface, fiber drawout, and fiber fracture.

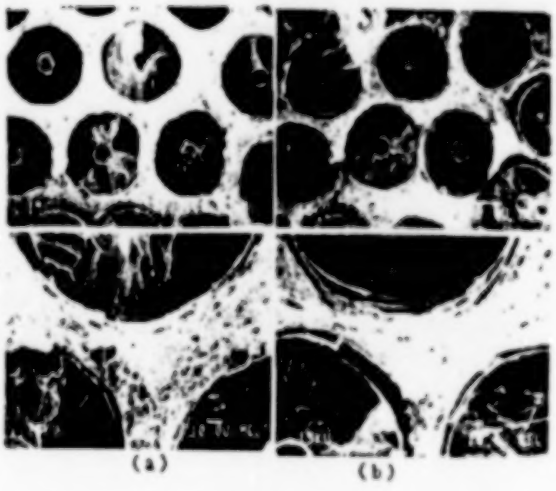

Figure 7. Fractograph of High-Temperature Tensile Fracture

4. Conclusion

Studies were conducted on the high temperature tensile strength test method in connection with evaluation of the mechanical characteristics of unidirectional continuous fiber reinforced metals at high temperature. Also, the high-temperature tensile strength characteristics in connection with the fracture mechanism were evaluated, and a simple method of measuring the stress-strain curve was developed.

A portion of this research was conducted as part of the Second-Term Quality Evaluation of Developed FRM in the "Research and Development of Composite Materials" based on the Project of Basic Technology for Future Industries by the Agency of Industrial Science and Technology, MITI. We express our thanks to those concerned with that portion of this research.

20158/9365

-END-

END OF FICHE DATE FILMED

9 November 88